CHAPTER 3

NULL SYNTHESIS

The desired omnidirectional radiation pattern with nulls can be obtained by using a null synthesis technique, which incorporates the characteristics of the conformal microstrip patches. In this chapter, three pattern synthesis techniques are used to form the desired null pattern.

Abele et al. [53] introduced a null synthesis technique for a cylindrical dipole array. The technique utilised the orthogonal projection method and projected an idealised null pattern onto the orthogonal base of realisable array patterns. The orthogonal projection method of Abele [53] is extended to include the radiation characteristics of microstrip patches mounted on a conducting cylinder. An idealised null pattern is then projected onto the space of realisable array patterns to obtain the element excitations.

The orthogonal projection method provides an optimal array pattern with the minimum pattern error (in a mean square sense). This implies that the amplitude and phase of the radiation pattern are optimised simultaneously, which may not provide the desired amplitude pattern characteristics. The Objective Weighting method, previously applied in other fields of computational electromagnetic problems [96, 97], is therefore used to improve the amplitude pattern characteristics. A global performance function is defined by utilising both the amplitude pattern error and the phase pattern error. This global performance function is then minimised by using the element excitations obtained from the orthogonal projection method as the starting values.

A constrained optimisation algorithm is also utilised to provide control over the individual amplitude pattern characteristics. The squared distance between the desired

pattern and the resulting pattern is minimised while constraining the characteristics of the amplitude pattern. The optimal element excitations provided by the orthogonal projection method are also used as starting values for the optimisation technique.

The null forming performance of the three techniques will be compared in this chapter. The resulting null patterns of the cylindrical microstrip patch array and an array of omnidirectional dipole elements are also compared. Furthermore, the influence of the array geometry (e.g. inter-element spacing and number of elements) and element radiation pattern on the amplitude pattern characteristics, are investigated.

3.1 Orthogonal projection method

3.1.1 Modification of the orthogonal base

The orthogonal projection method for equally spaced antenna elements, may be extended to include the radiation pattern of a conformal microstrip patch antenna. The extension is done by modifying the orthogonal base for the space of realisable array patterns given by $g_m(\phi)$, which is defined in Equation 2.43. The omnidirectional radiation pattern of the n-th antenna element is replaced with the directional radiation pattern of a cylindrical microstrip patch antenna. A similar technique was proposed by Vescovo [56] for an arc array of theoretical directional antenna elements. An element pattern can not be factorised out of the array pattern to obtain an array factor, since all the element patterns point in different directions. Once the orthogonal base has been extended, the unconstrained optimum sequence excitations are obtained from the projection of the ideal null pattern, $F_0(\phi)$, in Equation 2.39 onto the orthogonal base using Equation 2.46.

The element pattern may be obtained from either simulation or measurement. The projection method does not consider the mutual coupling between the antenna elements and it is also assumed that the antenna elements do not disturb each other's current distributions. Each element radiation pattern is thus identical to the radiation pattern of an isolated antenna in both shape and strength. The input impedance of each antenna element is furthermore assumed to be matched to the impedance of its port in the feeding network.

For electrically thin patch antennas, the cavity model have been shown to be sufficient to compute the characteristics of the patch antenna [23, 24, 29]. The two components of the radiation pattern, using the cavity model, are defined in Equations 2.10 and 2.11. To improve the bandwidth and gain performance, electrically thick patches are usually considered. For these electrically thick patches, hybrid modes are excited, which are neither pure TE nor TM polarized waves and require more accurate analysis methods [14]. The characteristics of these patches are therefore obtained from a finite difference time domain (FDTD) analysis program [30]. An infinitely long cylinder is considered in the cavity model and the effect of the edges of the cylinder on the radiation pattern are thus neglected [13]. The FDTD software may also be used to incorporate the effects of finite cylinders. Since the co-polar component will be used to form the desired radiation pattern, the element radiation pattern will refer only to the co-polar component of the radiation pattern of the patch antenna element.

3.1.2 Results of the projection method

The geometries of probe-fed axially and circumferentially polarised patch antenna arrays are used to illustrate the performance of the null synthesis method. The results are also compared with the results obtained with the null synthesis algorithm for omnidirectional element arrays. A cylindrical dipole array is used as a representative example.

Figure 3.1 illustrates the configuration of a typical cylindrical patch array, with d_ϕ and s_ϕ being the inter-element and edge spacing, respectively. Electrically thin conformal microstrip patches were designed for a resonant frequency of 1.8 GHz for the dominant mode, using $h = 0.159$ cm and $\varepsilon_r = 2.3$. $L = 2b = 5.44$ cm and $W = 2\theta_0 = 6$ cm for the axially polarised patches and $W = 2b = 6$ cm and $L = 2\theta_0 = 5.44$ cm for the circumferentially polarised patches. For the first example, six elements and an inter-element spacing of $d_\phi = 0.5\lambda_0$ was used. A null of infinite depth at 180° was desired. Therefore, an ideal null pattern with an abrupt phase reversal at 180° was projected onto the orthogonal base formed by the six element patterns. The unconstrained optimum sequence excitations obtained from the projection method, are then multiplied with a Hamming window to reduce the ripple in the omniregion, as proposed by Abele *et al* [53, 54]. The resulting sequence excitations are used to calculate the element excitations through the DFT relation in Equation 2.28.

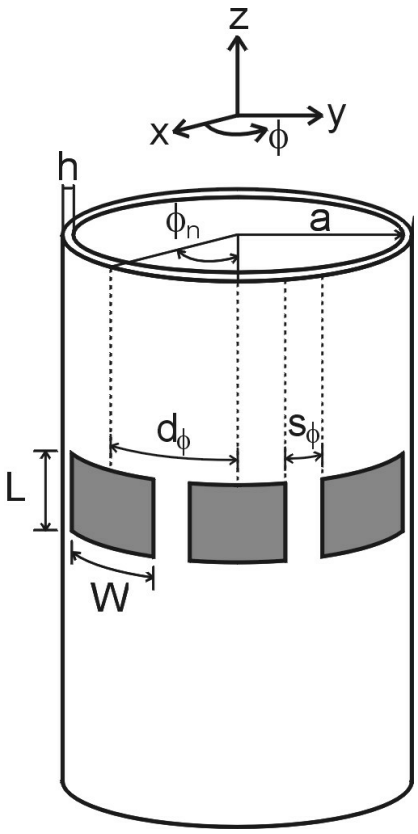

Figure 3.1: Configuration of a typical cylindrical microstrip patch antenna array

The array radiation patterns in Figure 3.2 were formed using the resulting element excitations for the axially and circumferentially polarised patch arrays. The radiation pattern obtained for a dipole array with the same number of elements and inter-element spacing is also shown for comparison. When comparing the nulls formed at 180° by the three cylindrical array configurations, it is seen that the resulting null characteristics are different. The circumferentially polarised patch array forms the deepest null with the least ripple, while the smallest null width is given by the axially polarised patch array. The differences in the resulting ripple and null widths are mainly due to the different antenna element patterns. The arrays with directional patch elements yielded better results than the array with omnidirectional dipole elements. Figure 3.3 also compares the phase of the resulting radiation patterns. All three phase patterns have an abrupt phase reversal at 180°, with the circumferentially polarised patch array having the least ripple in its phase pattern.

The number of elements of the arrays were increased to $N = 10$, while keeping the $0.5\lambda_0$ inter-element spacing. The same null with an infinite depth at 180° was required.

Figures 3.4 and 3.5 respectively compare the resulting amplitude and phase patterns of the projection method for the three arrays. Due to the increase in the degrees of freedom, the differences in the characteristics of the resulting null patterns of the arrays are less. A higher slope in the phase reversal and a decrease in ripple and null width are also observed for the increase in the number of array elements. The deepest null with the least ripple is formed by the circumferentially polarised patch array, while the smallest null width is obtained with the dipole array.

To study the influence of the number of array elements on the characteristics of the nulls, obtained with the projection method, the inter-element spacing was kept constant at $0.5\lambda_0$, while varying the number of elements ($6 \leq N \leq 20$). A null of infinite depth in the direction of the first element ($\phi_n = 2\pi/N$) was required. For each of the three array configurations, the gain ripple, null width and null depth are compared in Figures 3.6, 3.7 and 3.8, respectively. A gradual decrease in the ripple and null width is observed for the circumferentially and axially polarised patch arrays as the number of elements is increased. The null width of the resulting null patterns of the three arrays also become similar for a large number of elements ($N \geq 15$). When using the dipole array, a high gain ripple is observed for certain numbers of elements (e.g. $N = 11$ and $N = 14$). The high level of the ripple is due to the interference between dipole elements opposite each other in the cylindrical array. For a given array radius and a number of array elements, two dipole elements opposite each other can interfere strongly because of their omnidirectional radiation patterns. Consequently, the distortion in the dipole array patterns inhibits a smooth decrease in the gain ripple and null width as the number of elements is increased. On the other hand, the microstrip patches have directive radiation patterns and the ripple in the omnidirectional pattern is thus less. Figure 3.8 shows that maximum null depths are obtained with $N = 9$ and $N = 11$ for the axially and circumferentially polarised patch arrays, respectively. When a cylindrical dipole array is used, a maximum null depth may be obtained with $N = 19$.

While keeping the number of array elements constant at $N = 10$, the inter-element spacing was varied, yielding the results for the ripple, null width and null depth in Figures 3.9, 3.10 and 3.11, respectively. An omnidirectional array pattern with a single infinitely deep null at 180° was desired for all three array configurations. Using the circumferentially polarised patch array, a smooth increase in gain ripple is observed as the inter-element spacing is increased. Except for the abrupt increase in the ripple at $d_\phi = 0.625\lambda_0$, the ripple also increases smoothly as the inter-element spacing is

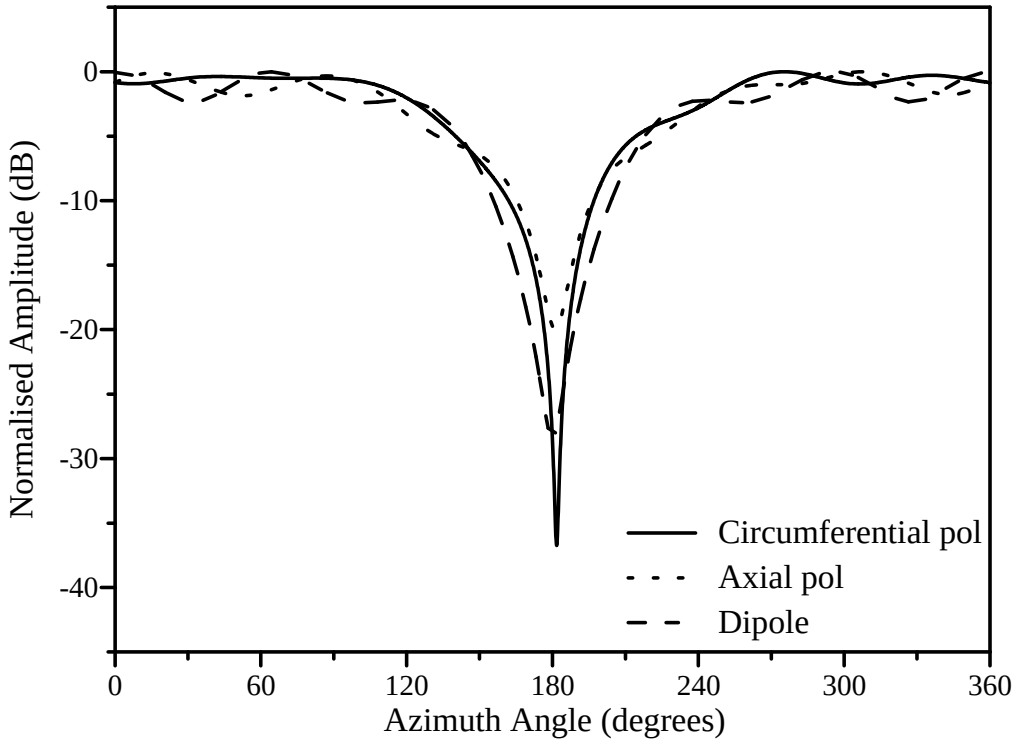

Figure 3.2: Radiation pattern of a cylindrical array (N=6 and $d_\phi = 0.5\lambda_0$) with a single null

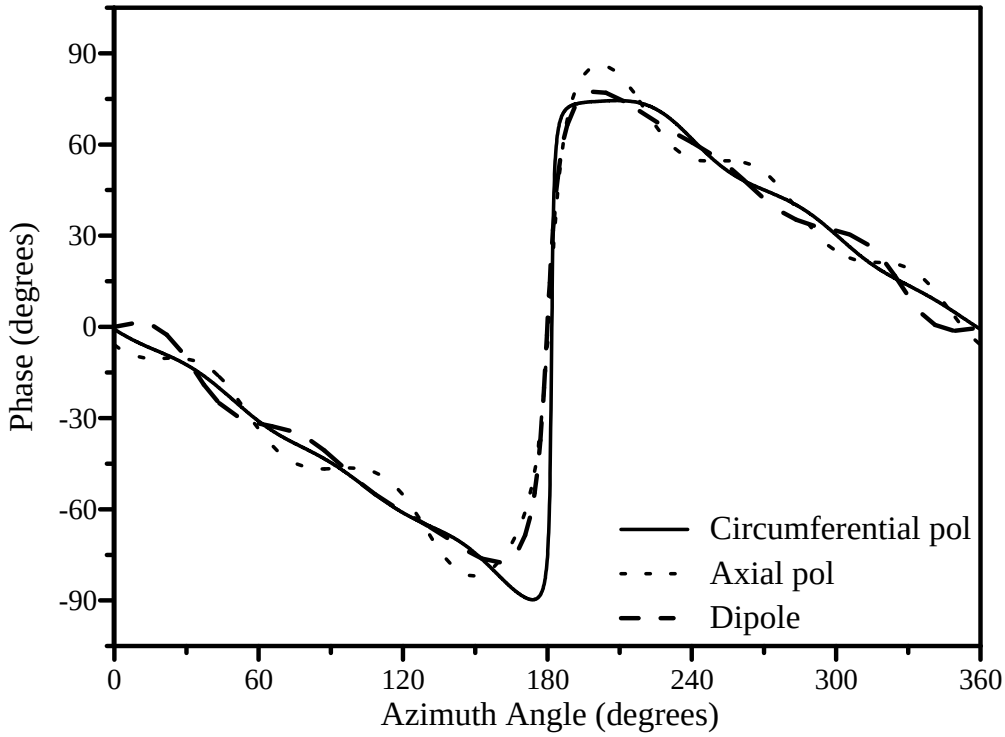

Figure 3.3: Phase of the radiation pattern for a cylindrical array (N=6 and $d_\phi = 0.5\lambda_0$) with a single null

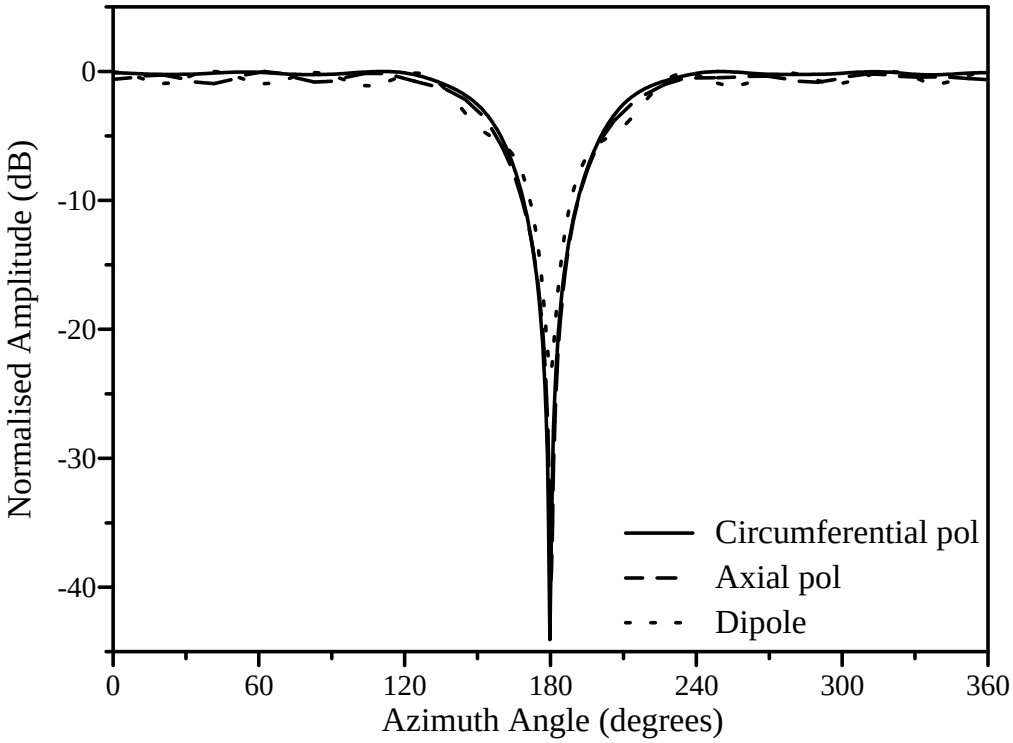

Figure 3.4: Radiation pattern of a cylindrical array (N=10 and $d_\phi = 0.5\lambda_0$) with a single null

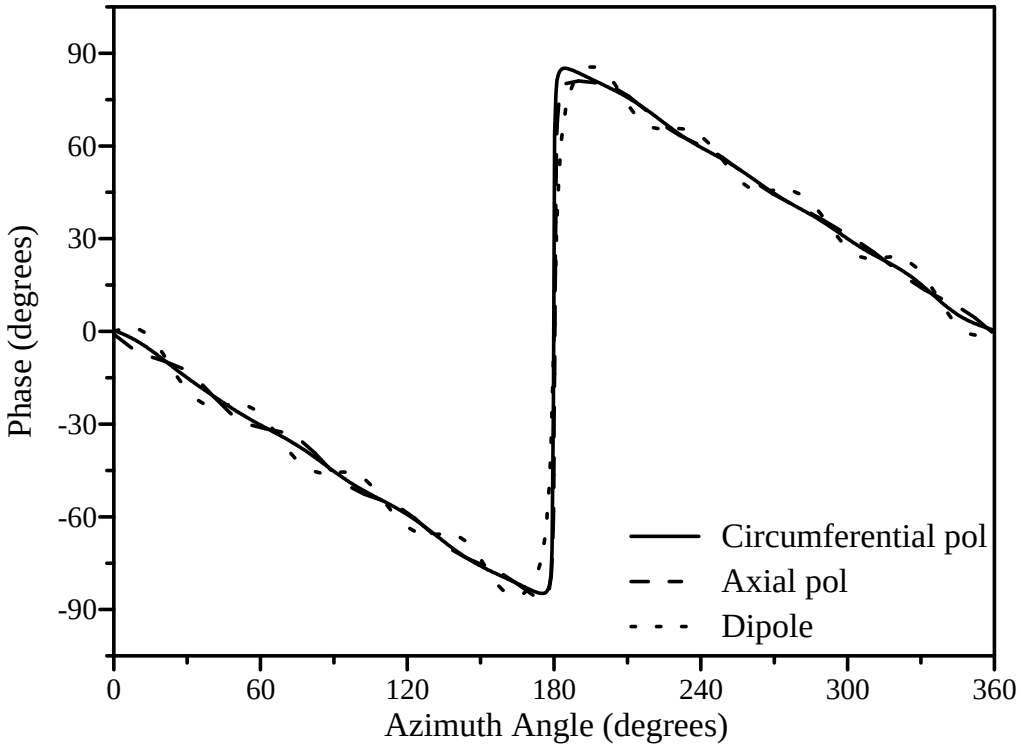

Figure 3.5: Phase of the radiation pattern for a cylindrical array (N=10 and $d_\phi = 0.5\lambda_0$) with a single null

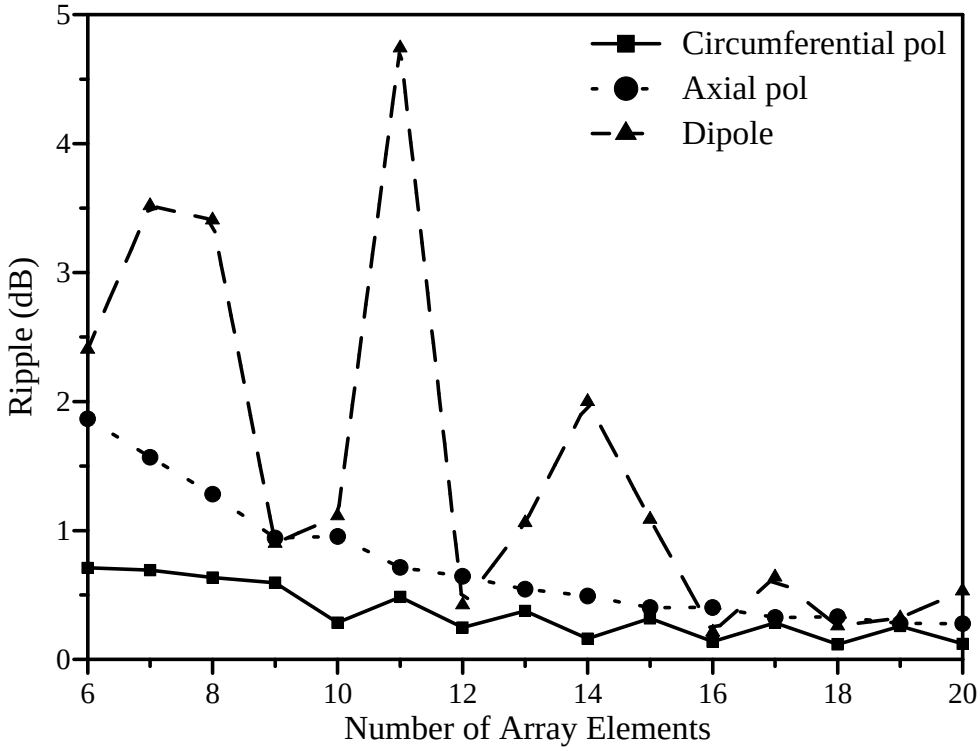

Figure 3.6: Resulting ripple of a single null in the radiation pattern of a cylindrical array with $d_\phi = 0.5\lambda_0$

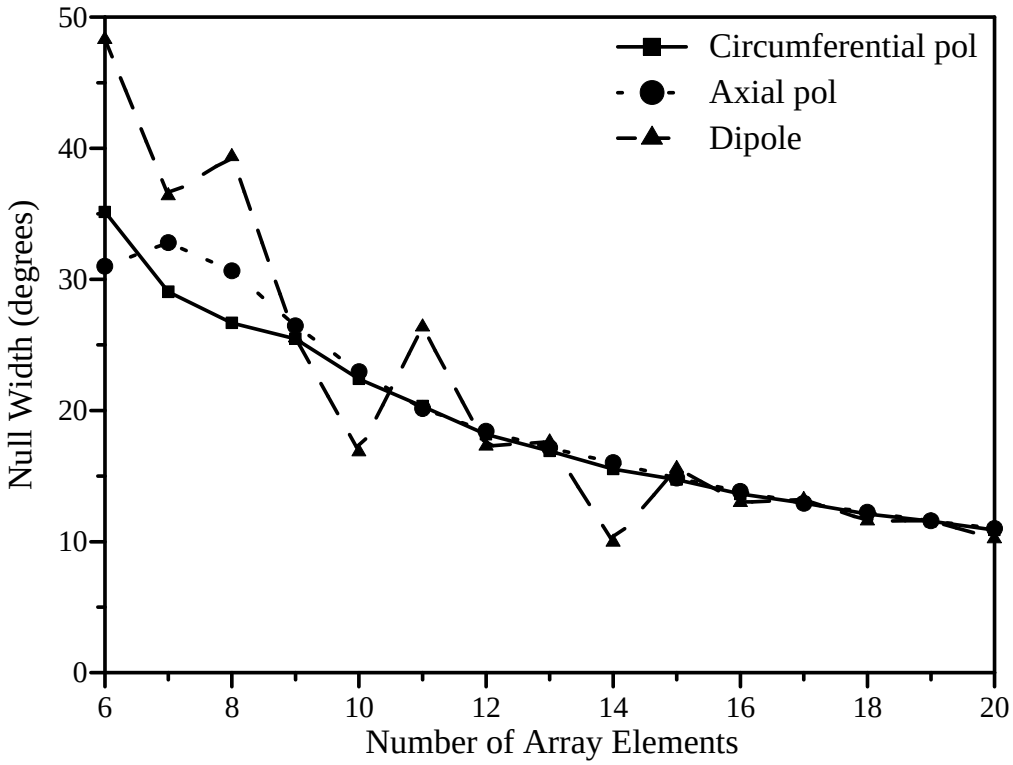

Figure 3.7: Resulting null width of a single null in the radiation pattern of a cylindrical array with $d_\phi = 0.5\lambda_0$

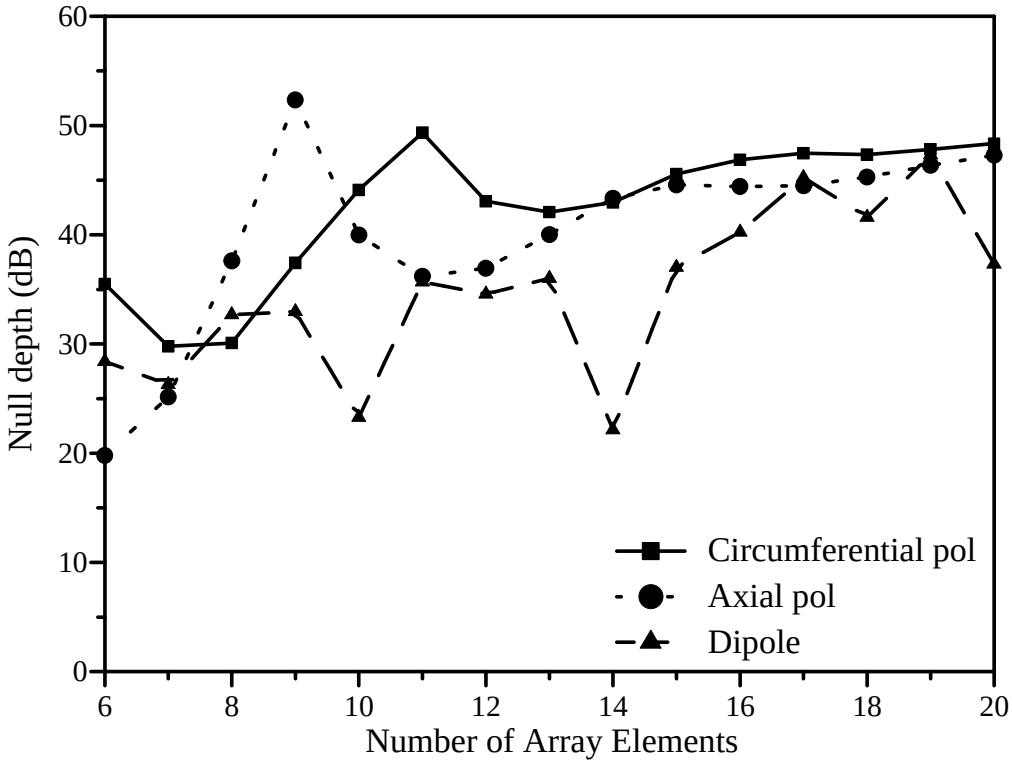

Figure 3.8: Resulting null depth of a single null in the radiation pattern of a cylindrical array with $d_\phi = 0.5\lambda_0$

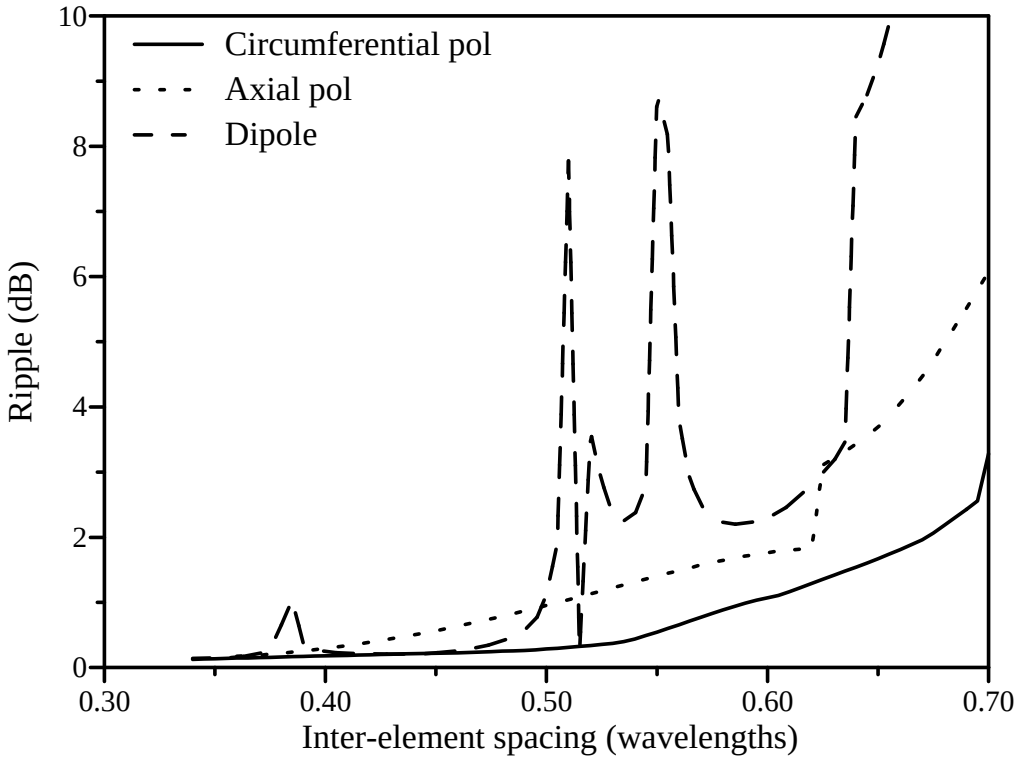

Figure 3.9: Resulting ripple of a single null in the radiation pattern of a cylindrical array with $N = 10$

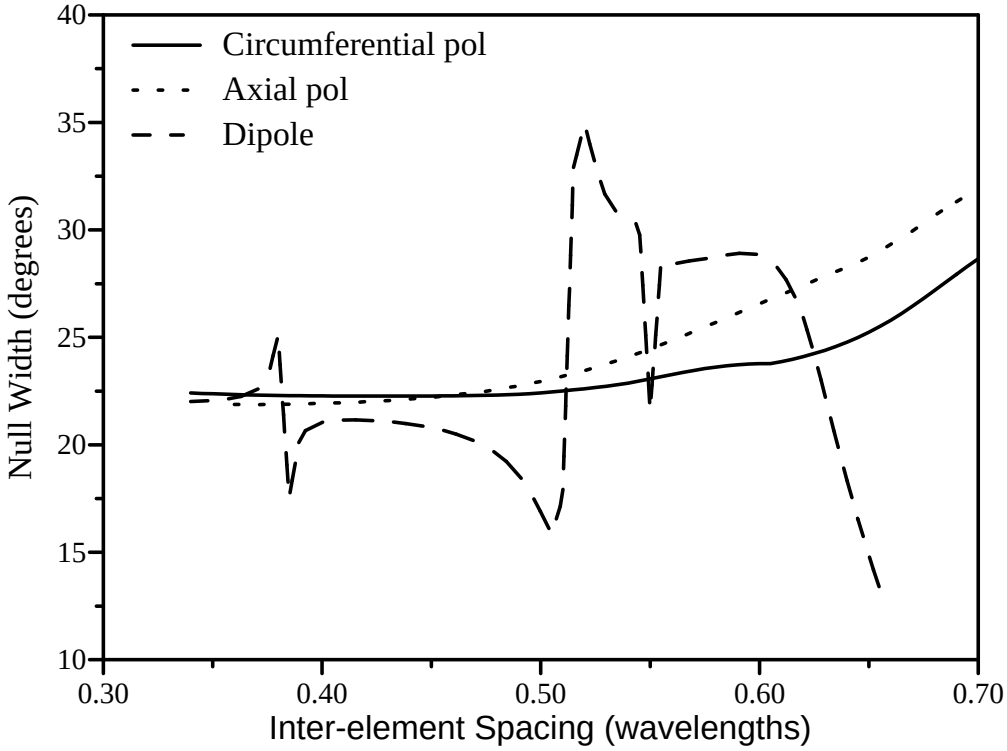

Figure 3.10: Resulting null width of a single null in the radiation pattern of a cylindrical array with $N = 10$

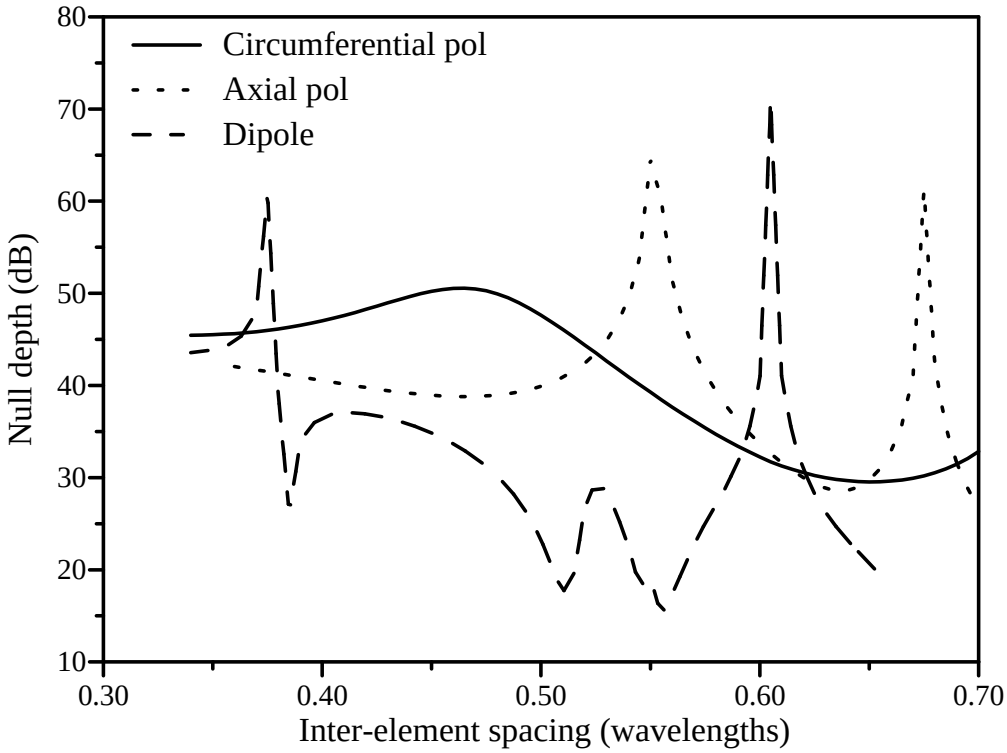

Figure 3.11: Resulting null depth of a single null in the radiation pattern of a cylindrical array with $N = 10$

increased in the axially polarised patch array. In contrast to the behaviour of the patch arrays, the gain ripple in the amplitude pattern of the dipole array depends highly on the inter-element spacing. For certain inter-element spacings, the interference between the elements yields large gain ripple values.

Figure 3.10 shows that the null widths of the resulting nulls increase gradually as the inter-element spacing is increased in both patch arrays. On the other hand, the utilisation of the dipole array may result in a maximum or minimum null width, depending on the inter-element spacing. All three arrays yield different null depth results using the orthogonal projection method, as seen in Figure 3.11. A maximum null depth of 49 dB at $d_\phi = 0.465\lambda_0$ may be obtained with the circumferentially polarised patch array. With the axially polarised patch array a maximum null depth of 64 dB can be obtained at $d_\phi = 0.55\lambda_0$, while the dipole array yields a maximum null depth of 71 dB at $d_\phi = 0.61\lambda_0$.

3.2 Objective weighting method

The orthogonal projection method provides an optimal array pattern with the least pattern error (in a least square sense). The optimal array pattern may not have the desired pattern characteristics, since the amplitude and phase of the radiation pattern are optimised simultaneously. Some of the amplitude pattern characteristics may be improved by applying a windowing function to the resulting element excitations. While some characteristics may improve, other characteristics are degraded.

This implies that a multi-objective optimisation approach has to be followed. In stead of minimising the array pattern error, a global performance function can be defined by utilising the amplitude pattern error and the phase pattern error. The minimum of this performance function is then sought after.

3.2.1 Performance function and Pareto optimality

In the objective weighting method a global performance function is obtained by means of a linear combination of the multi-objective functions of the optimisation scenario [97].

The performance function for an array pattern may be defined as:

$$P = c_1 e_a + c_2 e_p, \tag{3.1}$$

where c_1 and c_2 are weighting factors and e_a and e_p are the amplitude and phase pattern errors, respectively. The amplitude pattern error e_a is defined as:

$$e_a(\mathbf{A}) = \int_0^{2\pi} \left(|F(\phi;\mathbf{A})| - |F_0(\phi)|\right)^2 d\phi, \tag{3.2}$$

while the phase pattern error e_p is defined as:

$$e_p(\mathbf{A}) = \int_0^{2\pi} \left(\angle F(\phi;\mathbf{A}) - \angle F_0(\phi)\right)^2 d\phi. \tag{3.3}$$

The multi-objective optimisation problem can be solved by finding the minimum of P. Using the above definition, P will be independent of the minima of the objective functions e_a and e_p. It can also be observed from Equation 3.1, that the resulting values of e_a and e_p, which are obtained after finding the minimum of P, will depend on the ratio c_2/c_1. Thus, the ratio c_2/c_1 should be properly defined. The critical value of the ratio c_2/c_1 can be obtained through observing the behaviour of e_a and e_p when minimising different performance functions.

Figure 3.12 illustrates an example of an optimisation problem with different minima in a criterion space for different performance function definitions. The minima of P was found for different ratios c_2/c_1, which is indicated on the graph. For each minimum, the resulting values of e_a and e_p is shown. The curve formed by the resulting e_a and e_p is referred to as the Pareto optimal front which contains Pareto optimal points. A Pareto optimal point has been obtained when no other points exist in the variable domain for which the value of one of the two objective functions decreases and the other function does not increase [95–97]. The critical ratio (0.5), where $\sqrt{(e_a^2 + e_p^2)}$ is at a minimum, is circled on the graph. This Pareto optimal point is the most reasonable choice in a least square sense when trying to minimise both the amplitude and phase pattern errors.

The objective weighting method can thus be applied in a null synthesis technique to improve the amplitude pattern and consequently the amplitude pattern error. As indicated by the Pareto optimal front, the trade-off will be a gain in the phase pattern error for a loss in the amplitude pattern error.

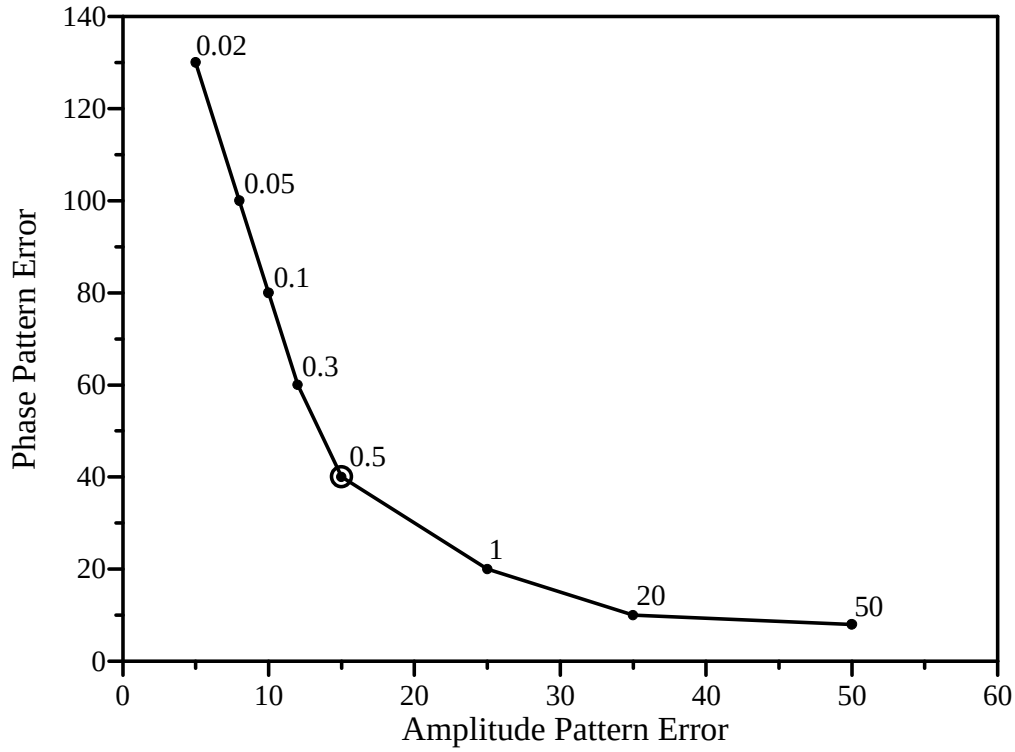

Figure 3.12: Example of different minima in a criterion space for different definitions of the performance function

The method is applied after the optimum element excitation vector $\mathbf{A}$ has been obtained from the projection method. An unconstrained non-linear minimisation algorithm [99] is used to find the minimum of each performance function P using this excitation vector as the starting vector. The algorithm applies a quasi-Newton optimisation method which incorporates a cubic-quadratic polynomial line search method. For each array configuration, the critical ratio c_2/c_1 and consequent function P has to be found. The excitation vector which minimises this P, is then used to form the omnidirectional radiation pattern with a null. In the next subsection, the objective weighting method is applied using the resulting excitation vectors of the projection method described in the previous section.

3.2.2 Results of the objective weighting method

The objective weighting method is applied using the unconstrained optimum excitation vectors obtained from the orthogonal projection method as starting values. The minima of P with different weight ratios are found using an unconstrained least square

optimisation algorithm. Figures 3.13 and 3.14 show examples of the Pareto optimal fronts for an axially and a circumferentially polarised patch array, respectively. The Pareto optimal fronts are shown for arrays with $N = 10$ and $d_\phi = 0.5\lambda_0$. An omnidirectional radiation pattern with a single infinitely deep null at 180° was required. In Figure 3.15 the optimal front for a dipole array with the same array configuration is shown. The objective weight ratios for each P is indicated along each point and the critical ratios are circled on all three graphs. For these array configurations, the axially and circumferentially polarised arrays have the same critical ratio of $c_1/c_2 = 0.1384$, while the dipole array has a critical ratio of $c_1/c_2 = 0.5904$.

After obtaining the excitations vectors which minimise P at the critical ratios, the resulting amplitude radiation patterns in Figure 3.16 were formed. The circumferentially polarised patch array forms the null with the least ripple, whereas the axially polarised patch array forms the deepest null. When comparing the results in Figure 3.16 to the results of the projection method in Figure 3.4, one can observe the decrease in null width and the increase in null depth for all three array types. On the other hand, the ripple in the omniregion increased in all three patterns. In Figure 3.17 the phase of the radiation patterns are shown. The increase in the ripple of the phase pattern can be seen when this figure is compared to Figure 3.5. The objective weighting method thus decreases the amplitude pattern error while increasing the phase pattern error. This is due to the trade-off that exists between the two pattern errors for optimal points on the Pareto optimal front - a decrease in one objective will result in an increase in the other objective.

The resulting gain ripple, null width and null depth are compared for different numbers of array elements in Figures 3.18, 3.19 and 3.20, respectively. The inter-element spacing was kept constant at $d_\phi = 0.5\lambda_0$ and an infinitely deep null at 180° was required. The ripple in Figure 3.18 gradually decreases to a value close to 1 dB as the number of elements increases. This value is higher than the ripple of 0.5 dB or lower, which was obtained with the orthogonal projection method for $N = 20$ in Figure 3.6. The null width also decreases as the number of elements is increased. Compared to the results of the projection method in Figure 3.7, the objective weighting method forms nulls with smaller null widths. Figure 3.20 shows that deep nulls can be obtained by using only a small number of array elements. Using the projection method, as seen in Figure 3.8, lower null depths were obtained for small numbers of elements.

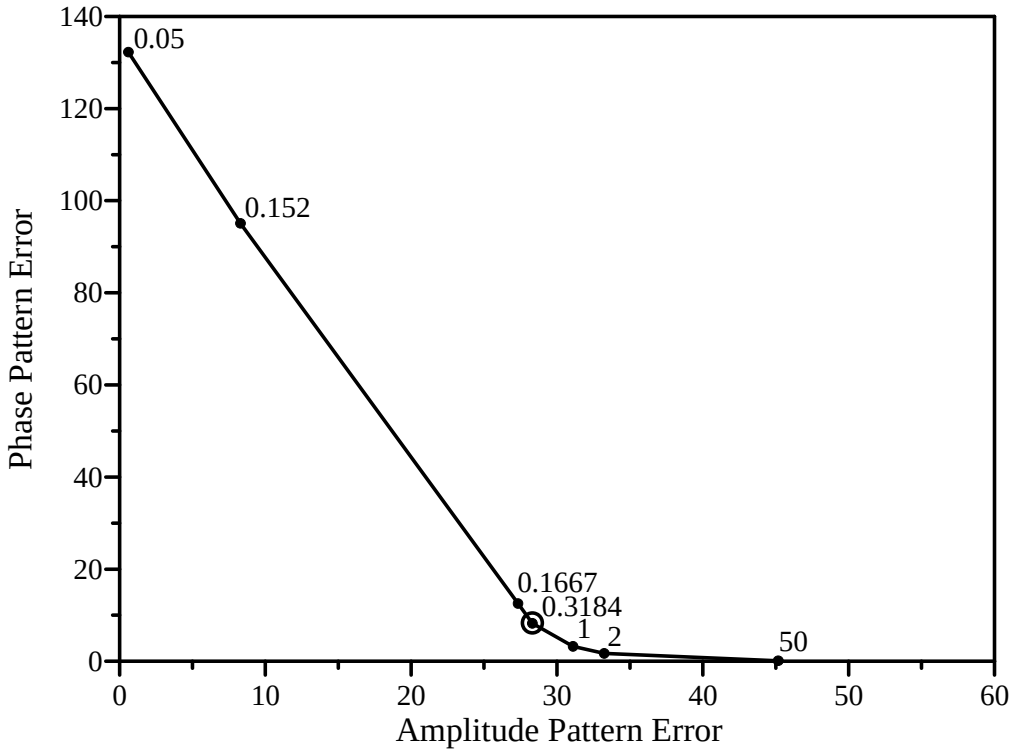

Figure 3.13: Minima for different definitions of the performance function for a cylindrical array of axially polarised patches with $N = 10$ and $d_\phi = 0.5\lambda_0$

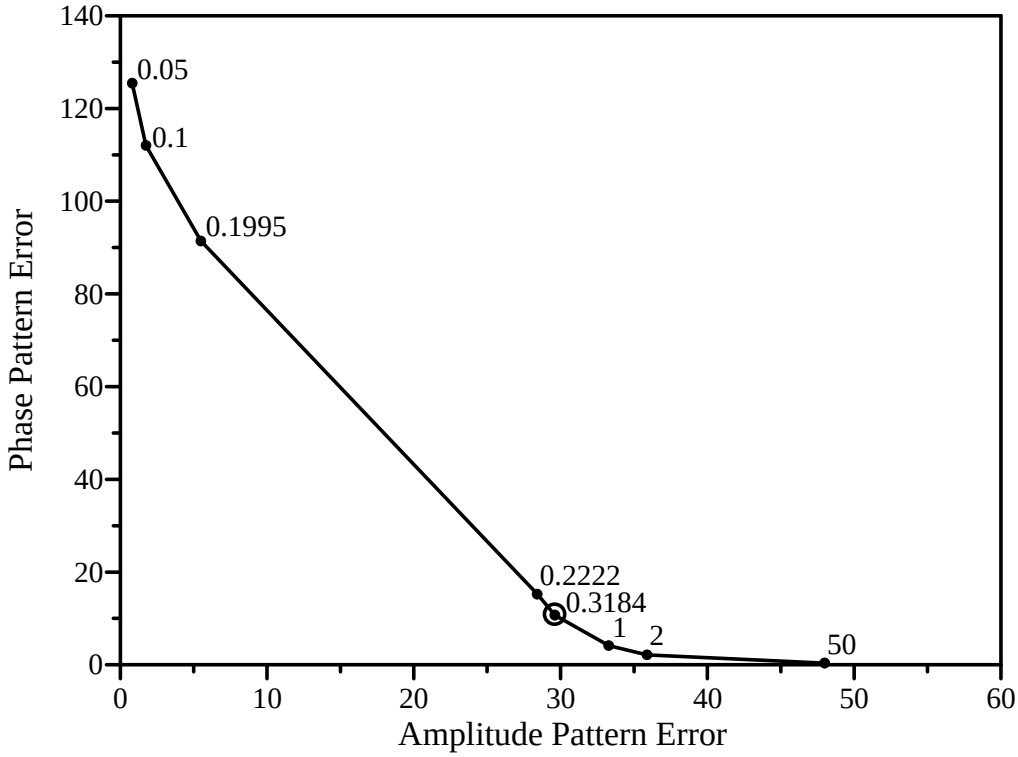

Figure 3.14: Minima for different definitions of the performance function for a cylindrical array of circumferentially polarised patches with $N = 10$ and $d_\phi = 0.5\lambda_0$

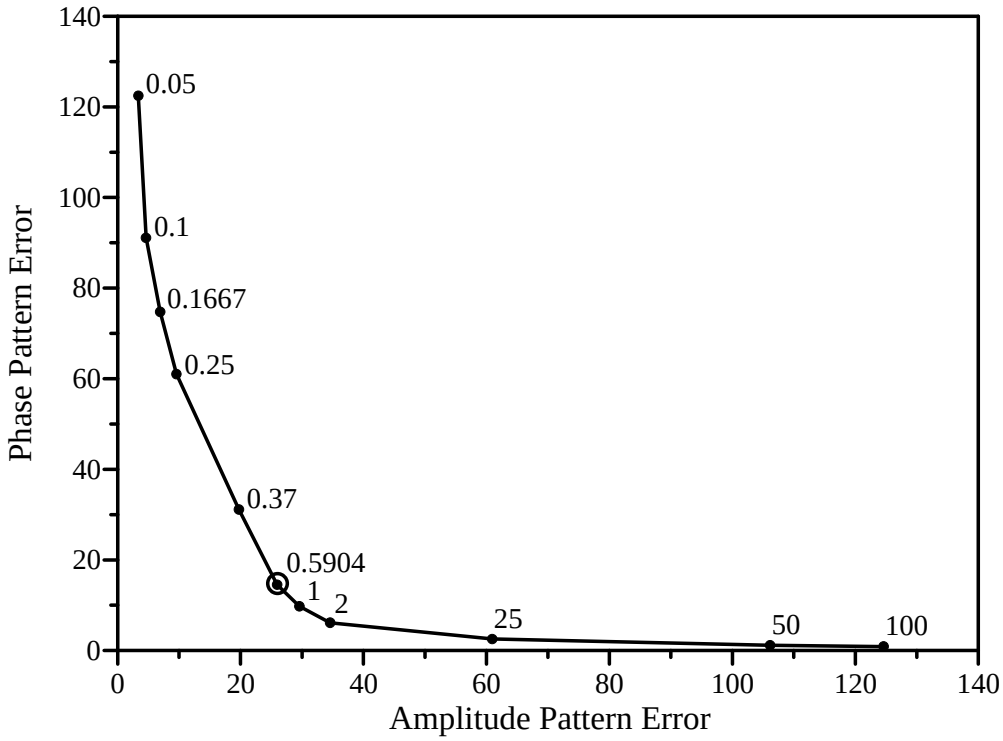

Figure 3.15: Minima for different definitions of the performance function for a cylindrical array of dipoles with $N = 10$ and $d_\phi = 0.5\lambda_0$

While keeping the number of array elements constant at $N = 10$, the inter-element spacing of the arrays was varied. The resulting ripple, null width and null depth are compared for the different types of arrays in Figures 3.21, 3.22 and 3.22, respectively. For the dipole array with $d_\phi = 0.55\lambda_0$, the objective weighting function could not yield a critical ratio value for P due to the high ripple in the omni-region. No results for this inter-element spacing could thus be shown in the figures.

For patch arrays with $d_\phi \geq 0.45\lambda_0$, the ripple increases as the inter-element spacing is increased in Figure 3.21. In Figure 3.22, the resulting null width for a circumferentially polarised patch array decreases as the inter-element spacing increases for $d_\phi \leq 0.55\lambda_0$. For $d_\phi \geq 0.6\lambda_0$, the null width starts to increase for increasing inter-element spacing. The null width for an axially polarised patch array firstly decreases with increasing inter-element spacing up to $d_\phi = 0.5\lambda_0$ before it increases for increasing inter-element spacing. Using the objective weighting method, maximum null depths can be obtained with inter-element spacings of $d_\phi = 0.625\lambda_0$ and $d_\phi = 0.675\lambda_0$ for circumferentially and axially polarised patch arrays, respectively.

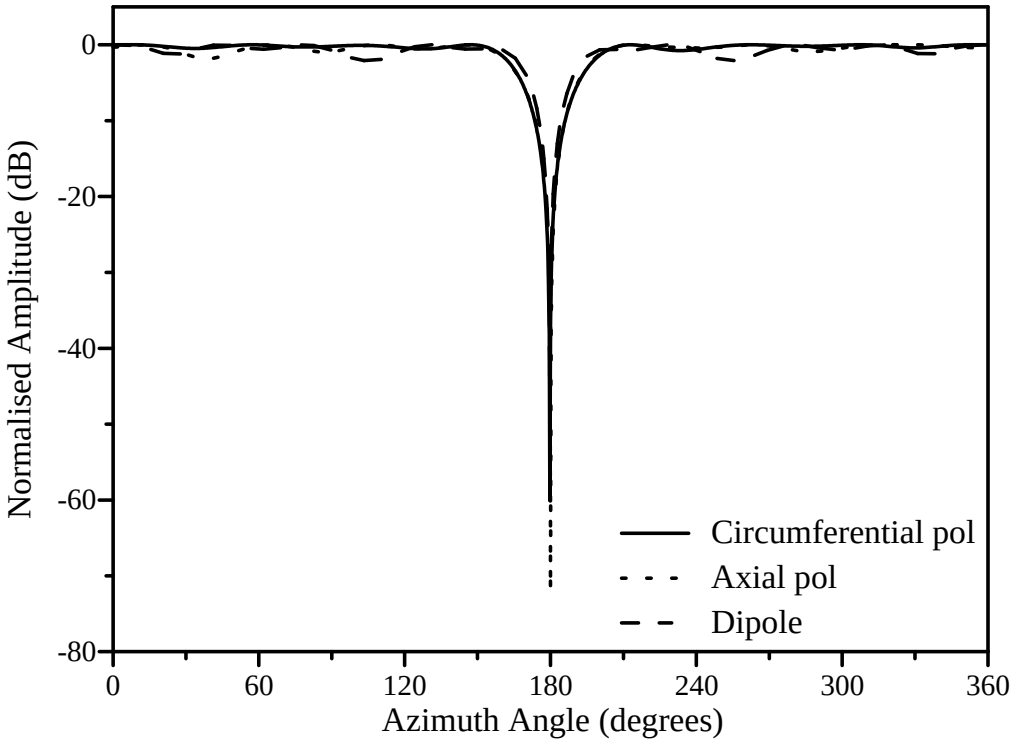

Figure 3.16: Radiation pattern of a cylindrical array (N=10 and $d_\phi = 0.5\lambda_0$) with a single null, using the objective weighting method

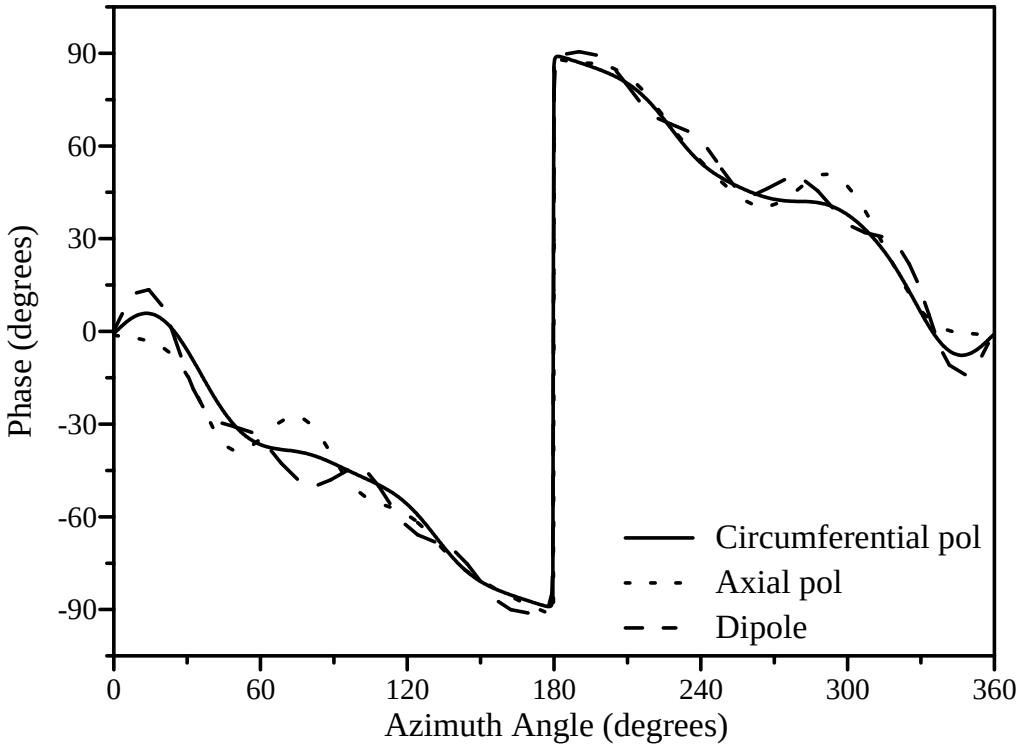

Figure 3.17: Phase of the radiation pattern for a cylindrical array (N=10 and $d_\phi = 0.5\lambda_0$) with a single null, using the objective weighting method

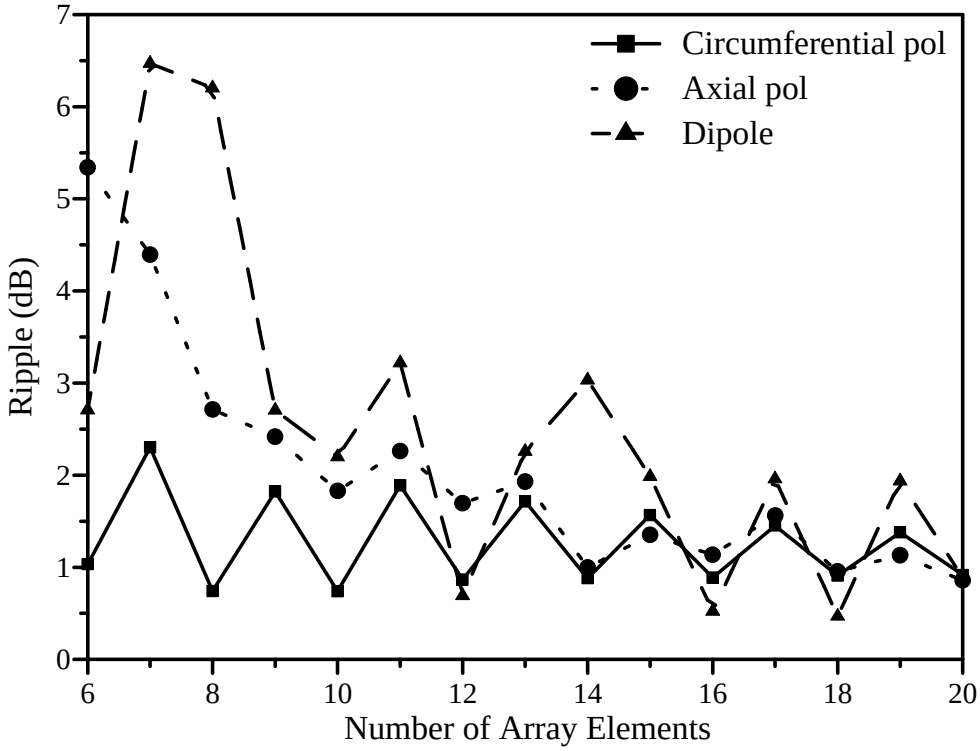

Figure 3.18: Resulting ripple of a single null in the radiation pattern of a cylindrical array with $d_\phi = 0.5\lambda_0$, using the objective weighting method

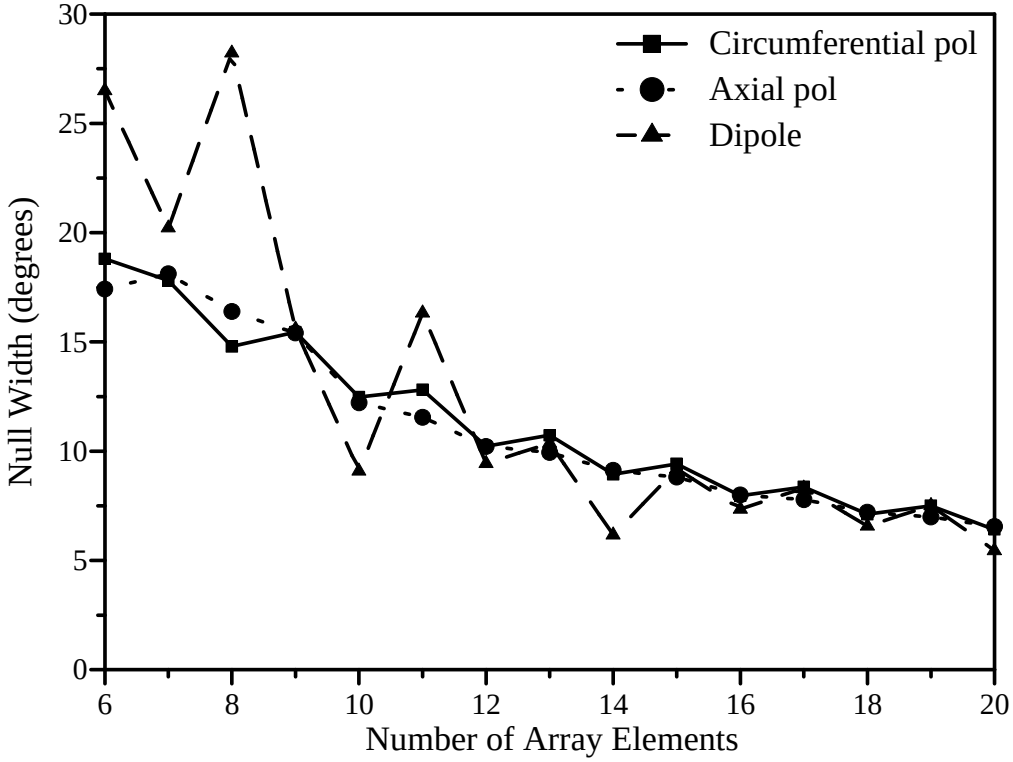

Figure 3.19: Resulting null width of a single null in the radiation pattern of a cylindrical array with $d_\phi = 0.5\lambda_0$, using the objective weighting method

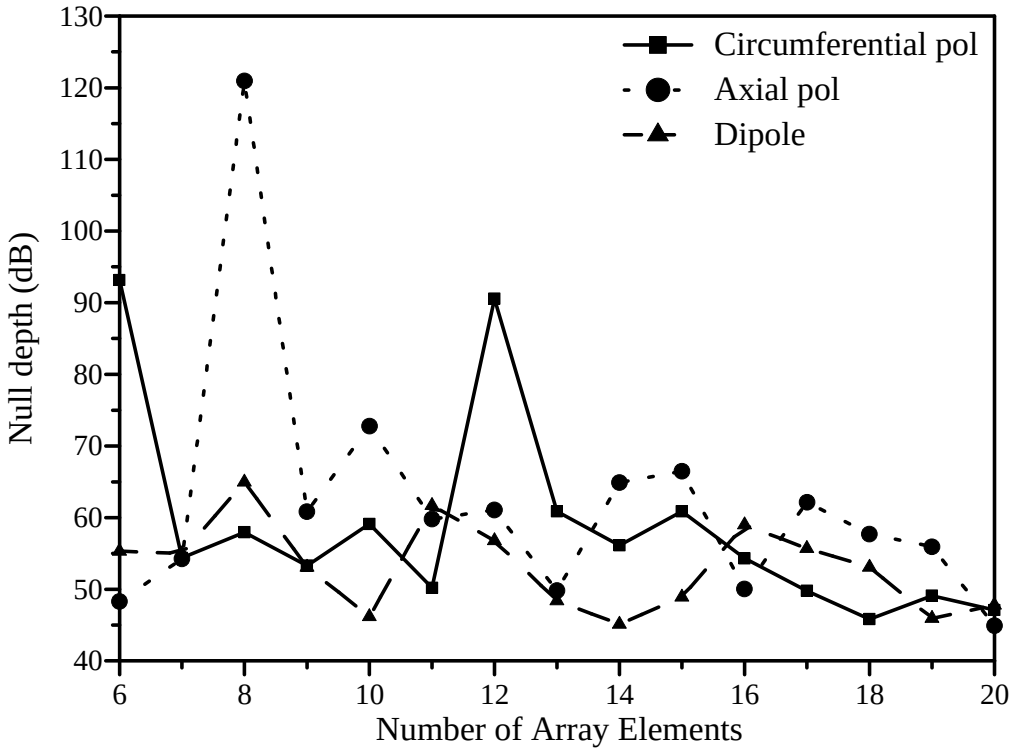

Figure 3.20: Resulting null depth of a single null in the radiation pattern of a cylindrical array with $d_\phi = 0.5\lambda_0$, using the objective weighting method

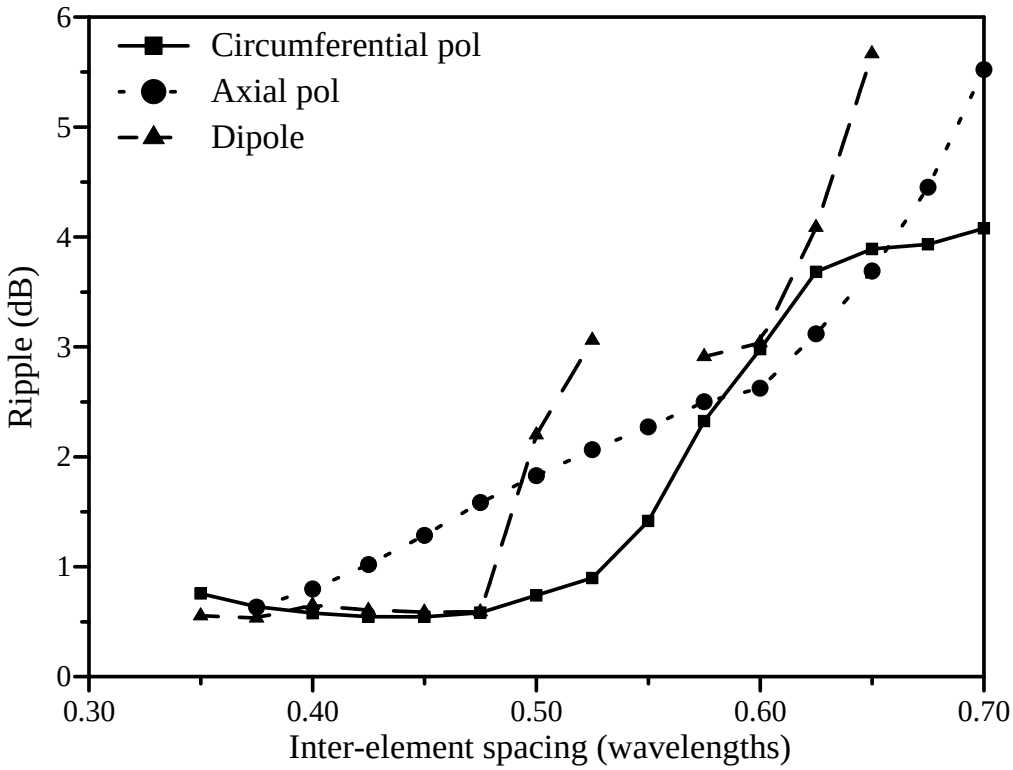

Figure 3.21: Resulting ripple of a single null in the radiation pattern of a cylindrical array with $N = 10$, using the objective weighting method

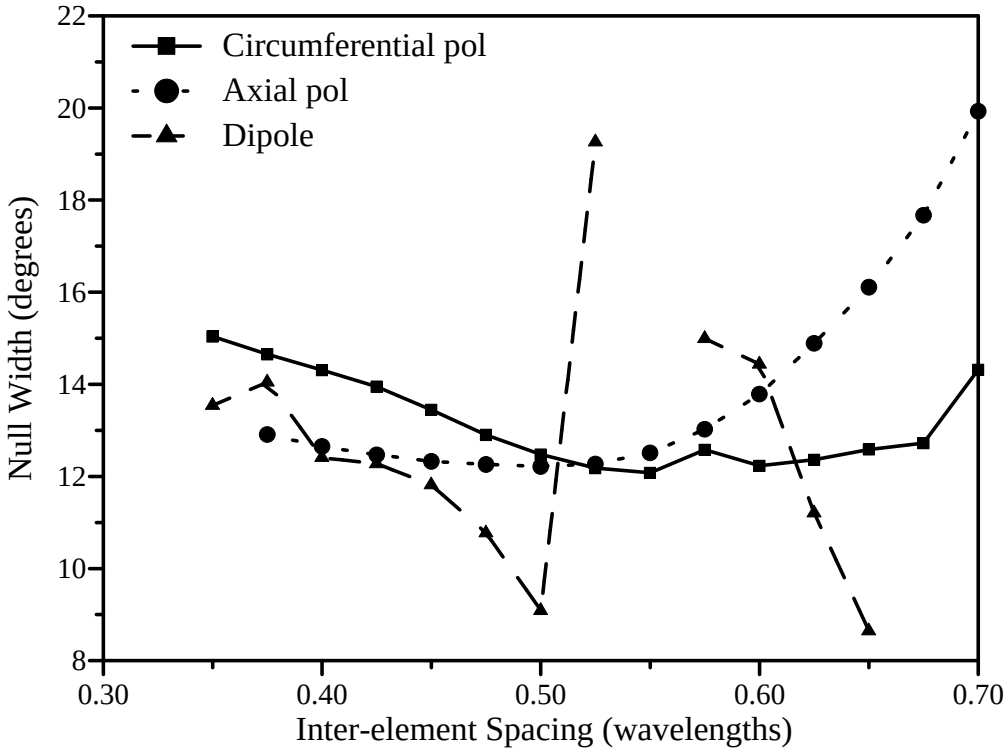

Figure 3.22: Resulting null width of a single null in the radiation pattern of a cylindrical array with $N = 10$, using the objective weighting method

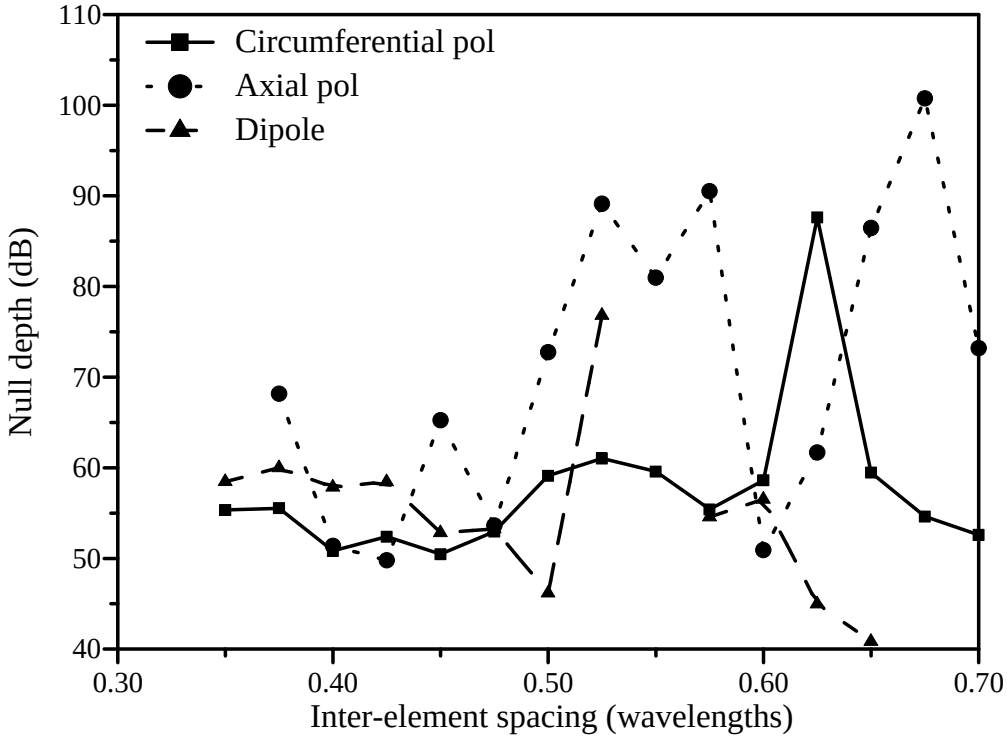

Figure 3.23: Resulting null depth of a single null in the radiation pattern of a cylindrical array with $N = 10$, using the objective weighting method

3.3 Constrained optimisation

The objective weighting method provides a way of improving the characteristics of the amplitude radiation pattern. This improvement is mostly manifested in a decreased null width and an increased null depth when an infinitely deep null is considered. On the other hand, the gain ripple in the omni-region increases.

Another way of improving the resulting amplitude pattern would be to provide control over the individual characteristics. In some applications, the degree of suppression needs to be specified through a controllable null depth. As discussed previously, Abele [54] proposed a variable phase step to provide control over the null depth. The accuracy of the resulting null depth depends on the array configuration and the desired null depth.

Constrained optimisation provides a method of constraining the different attributes of the amplitude pattern while minimising the array pattern error. All the attributes or combinations of attributes can thus be controlled.

3.3.1 Results of the constrained optimisation

A constrained optimisation algorithm [99] is employed to find an excitation vector which yields the minimum pattern error under the constraints specified for certain amplitude pattern characteristics. The choice of the starting values for the excitations vector fulfils a very important role in the success of the optimisation. When these values are chosen carefully, the optimisation time can be limited and local minima can be avoided. The excitation vector obtained from the orthogonal projection method yields an optimum radiation pattern with the minimum pattern error and is therefore chosen as the starting value. The resulting vector from the constrained optimisation will produce a radiation pattern with a pattern error as close as possible to this minimum pattern error while satisfying the constraints.

The algorithm allows the placement of constraints on the gain ripple, the null depth and the null width. These constraints are set equal to the desired values of the characteristics. Two additional constraints are also placed on the amplitudes and phases of the element excitations:

$$|a_n| \leq 1, \tag{3.4}$$

and

$$|\angle a_n| \leq 180°. \tag{3.5}$$

The above constraints effectively decrease the variable space to the normalised excitation amplitudes and one 360° phase cycle for the excitation phases. The execution time of the optimisation algorithm is consequently decreased.

Different combinations of constraints were used to illustrate the performance of the algorithm. The antenna element configuration of the previous sections was applied in a circumferentially polarised patch array. A -40 dB null at 180° was desired. The various constrained optimisation study cases and their results are summarised in Table 3.1. Figure 3.24 shows the resulting amplitude patterns for study cases 1 to 3, while the amplitude patterns of study cases 4 to 6 are shown in Figure 3.25. The amplitude pattern of the last study case is presented in Figure 3.26. Table 3.1 shows that either individual characteristics or combinations of characteristics are controllable using the constrained optimisation. When the ripple is not constrained to be 1 dB, the resulting ripple is between 1.63 and 1.72 dB. The unconstrained null depth is between -22.1 and -23 dB, while the unconstrained null width varies from 13.11° to 13.6°.

Table 3.1: Study cases for constrained optimisation

Case	**Constraints**			**Results**		
	Null depth (dB)	Ripple (dB)	Null width (°)	Null depth (dB)	Ripple (dB)	Null width (°)
1	-40	none	none	-40.0	1.70	13.54
2	none	1	none	-22.8	1	13.11
3	none	none	13	-23.0	1.63	13.00
4	-40	1	none	-40.0	1	13.60
5	none	1	13	-22.1	1	13.00
6	-40	none	13	-40.0	1.72	13.00
7	-40	1	13	-40.0	1	13.00

Case study 4 was extended to investigate the effect of different numbers of elements and inter-element spacings on the resulting unconstrained null width. Figure 3.27 compares the resulting null width for the different types of arrays as the number of elements is varied. The inter-element spacing was kept constant at $d_\phi = 0.5\lambda_0$. As the number of elements is increased while the desired null depth and ripple are constrained, the

null width gradually decreases. Arrays with an uneven number of elements produce wider null widths than arrays with an even number of elements for $N \geq 9$. The circumferentially and axially polarised patch arrays show similar null widths for $N > 11$, while for a large number of array elements ($N > 16$), the null widths of all three arrays become similar.

While keeping the number of elements constant at $N = 10$, the inter-element spacing was varied, yielding the results in Figure 3.28. Due to the high distortion in the far-field of the dipole array, a gain ripple of less than 1 dB could not be obtained with the dipole array, while the axially and circumferentially polarised patch arrays could not form the null with a 1 dB ripple for $d_\phi > 0.65\lambda_0$ and $d_\phi > 0.675\lambda_0$, respectively. The circumferentially polarised patch array patterns have the smallest null widths for $d_\phi > 0.5\lambda_0$.

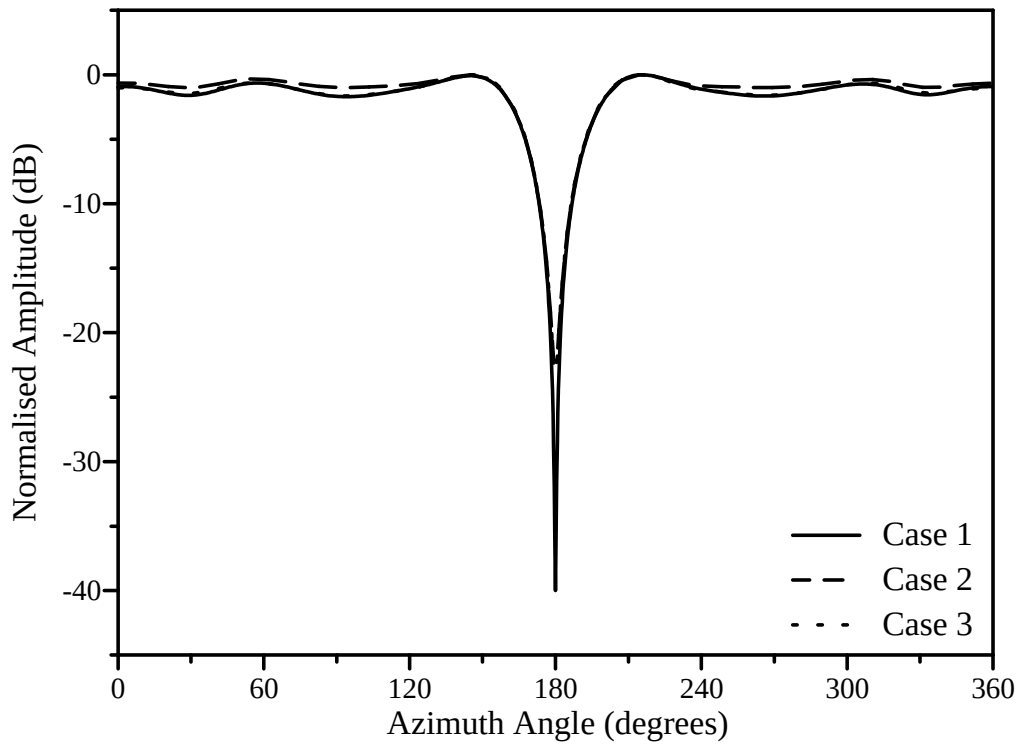

Figure 3.24: Radiation pattern of a cylindrical array (N=10 and $d_\phi = 0.5\lambda_0$) with a single null, using the constrained optimisation method for cases 1, 2 and 3

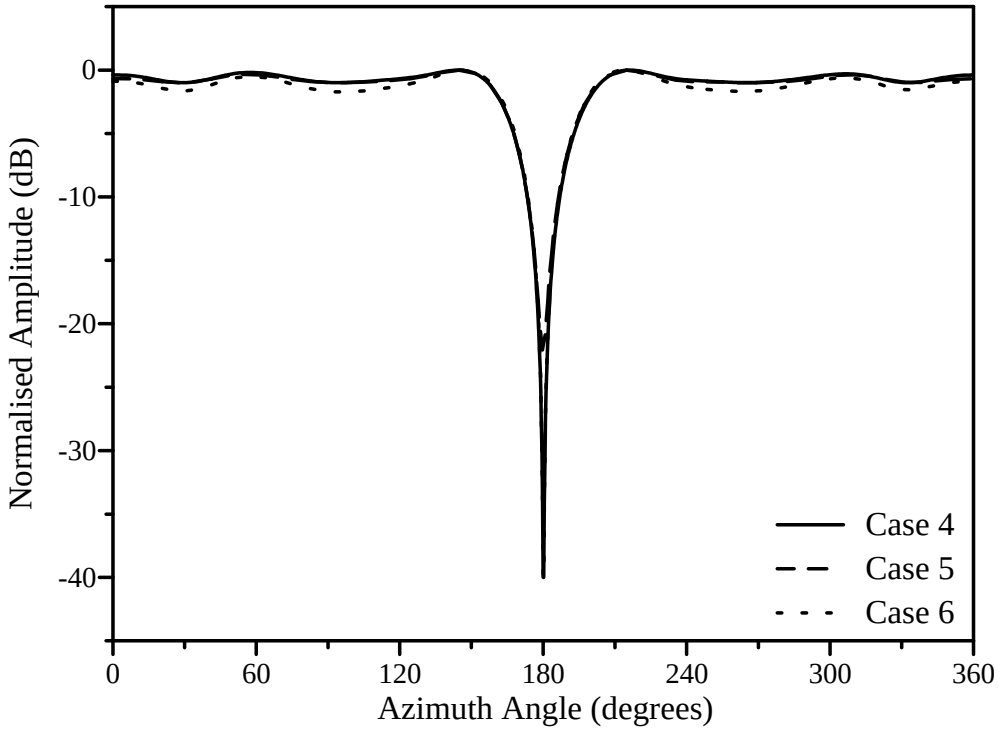

Figure 3.25: Radiation pattern of a cylindrical array (N=10 and $d_\phi = 0.5\lambda_0$) with a single null, using the constrained optimisation method for cases 4, 5 and 6

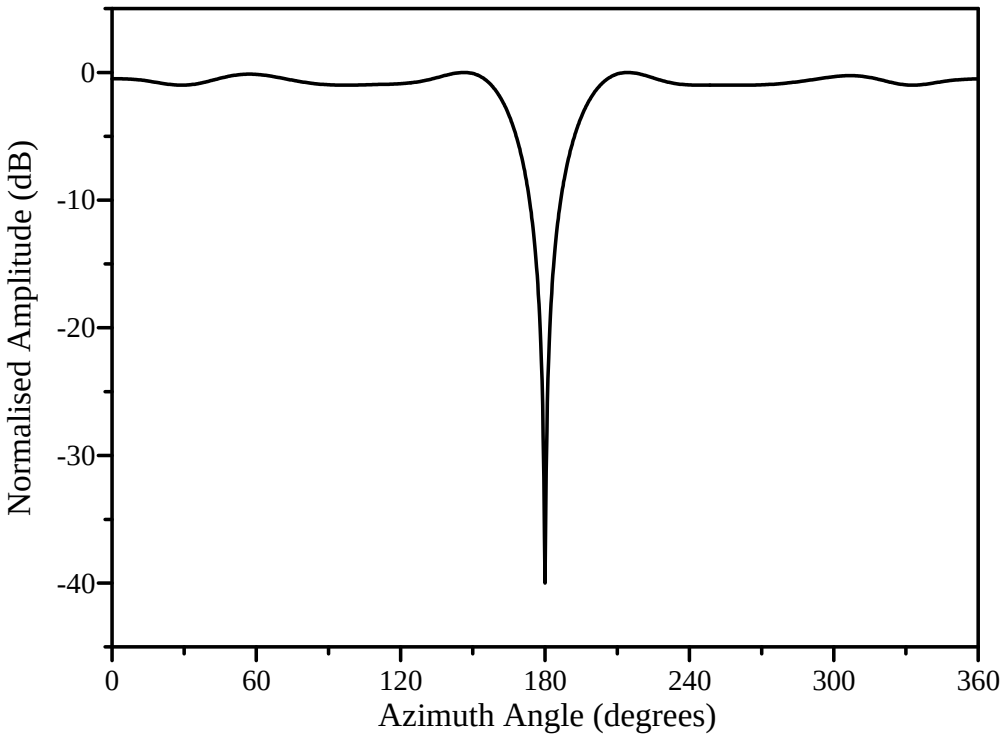

Figure 3.26: Radiation pattern of a cylindrical array (N=10 and $d_\phi = 0.5\lambda_0$) with a single null, using the constrained optimisation method for case 7

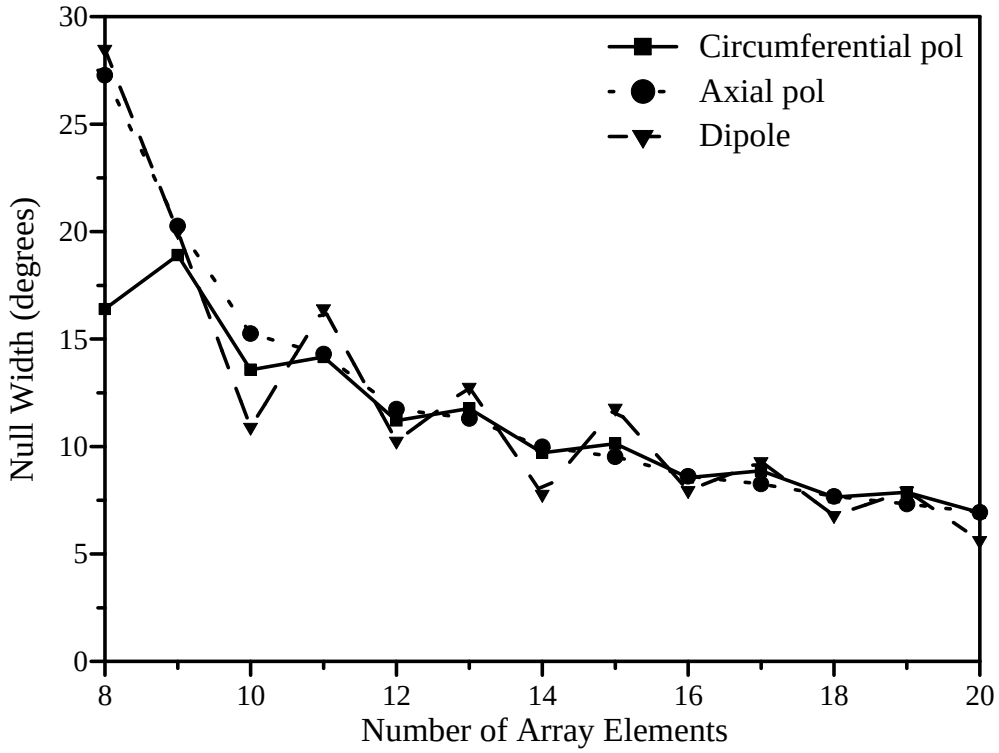

Figure 3.27: Resulting null width of a single null (40 dB depth, 1 dB ripple) in the radiation pattern of a cylindrical array with $d_\phi = 0.5\lambda_0$

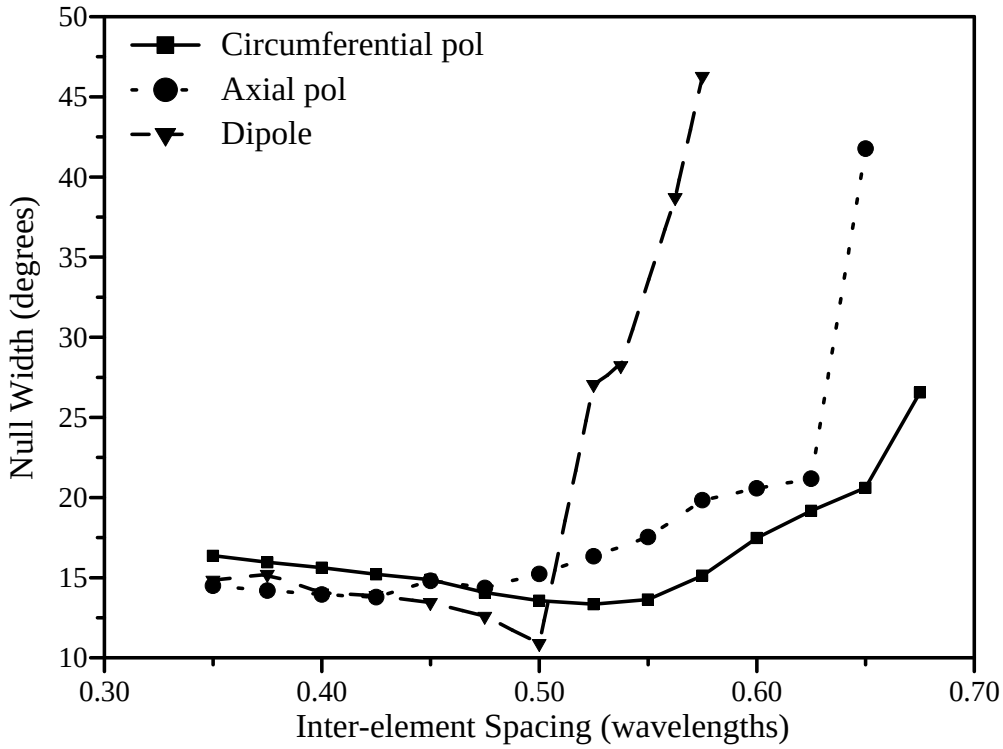

Figure 3.28: Resulting null width of a single null (40 dB depth, 1 dB ripple) in the radiation pattern of a cylindrical array with $N = 10$

3.4 Comparison of null synthesis methods

Each of the optimisation methods proposed in the previous sections have different advantages and disadvantages. To compare the results of the three methods, a single -40 dB null at 180° was specified as the desired null. The orthogonal projection method was used to obtain the starting excitation vector for all the methods. The results of the different optimisation methods for different types of arrays ($N = 10$ and $d_\phi = 0.5\lambda_0$) are compared in Table 3.2. In the first method, a window function was applied to reduce the ripple in the omni-region. Figures 3.29, 3.30 and 3.31 compare the resulting amplitude patterns of the first three optimisation methods for a circumferentially polarised patch array, an axially polarised patch array and a dipole array, respectively.

For each array configuration, the projection method forms the null with the least gain ripple, but with the largest null width. The objective weighting method produces a null with the least null width, but the resulting null is deeper than required. When the constrained method is used with only one constraint placed on the null depth, the resulting gain ripple for the patch arrays is higher than the gain ripple obtained from the projection and objective weighting methods. The obtained null width is also slightly higher than the null width produced by the objective weighting method. By constraining the ripple as well, the null width remains almost the same for the circumferentially polarised patch array, but slightly increases for the axially polarised patch array.

When only a low gain ripple is of concern, the orthogonal projection method with a window function can be used. On the other hand, the objective weighting method can be applied to obtain a narrow null when a higher gain ripple is tolerable. The resulting null depth for these two methods will depend on the number of elements as well as the inter-element spacing. The constrained optimisation method can be used to control both the null depth and the ripple, while obtaining a null width close to the null width resulting from the objective weighting method.

In the next section, the constrained optimisation method will be used to form multiple nulls in an otherwise omnidirectional pattern.

Table 3.2: Results of different optimisation methods for cylindrical arrays with $N = 10$ and $d_\phi = 0.5\lambda_0$

Array type	**Method**	**Null depth (dB)**	**Ripple (dB)**	**Null width (°)**
Circumferentially polarised patches	Projection with windowing	-36.1	0.27	22.31
	Objective weighting	-48.0	0.68	12.50
	Constraint: -40 dB	-40.0	1.70	13.54
	Constraints: -40 dB, 1dB ripple	-40.0	1.00	13.51
Axially polarised patches	Projection with windowing	-34.3	0.97	23.28
	Objective weighting	-81.9	1.85	12.21
	Constraint: -40 dB	-40.0	2.66	13.81
	Constraints: -40 dB, 1dB ripple	-40.0	1.00	15.25
Dipoles	Projection with windowing	-34.3	0.98	23.32
	Objective weighting	-46.5	2.05	9.10
	Constraint: -40 dB	-40.0	1.70	13.74
	Constraints: -40 dB, 1dB ripple	-40.0	1.00	10.89

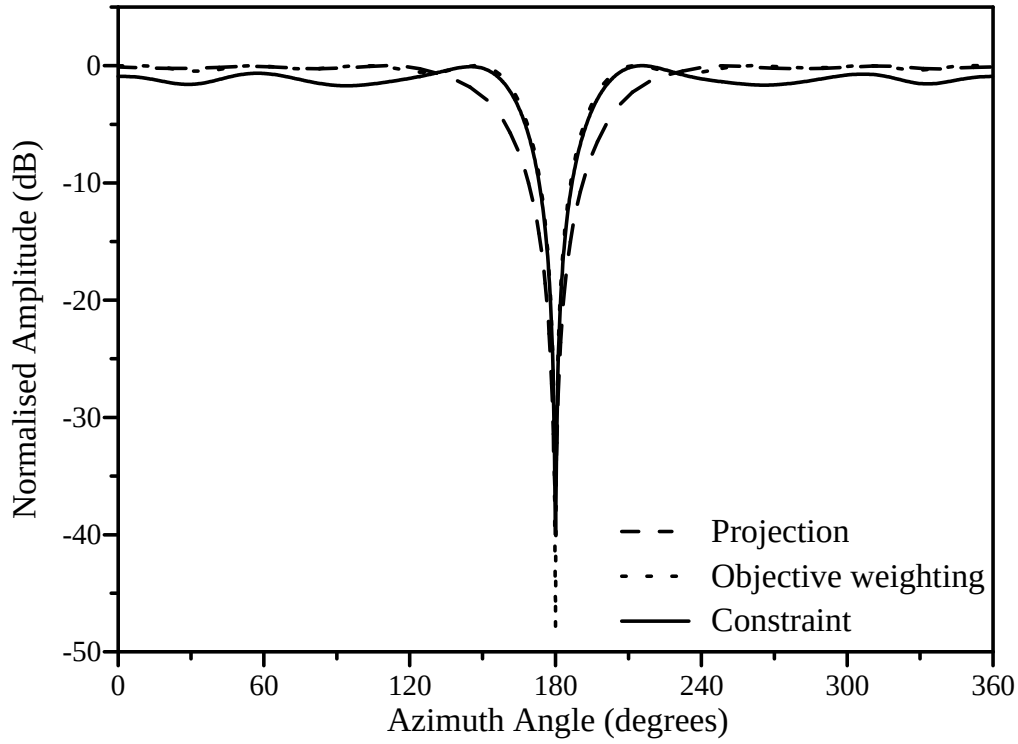

Figure 3.29: Radiation pattern of a circumferentially polarised patch array (N=10 and $d_\phi = 0.5\lambda_0$) with a single null using different methods

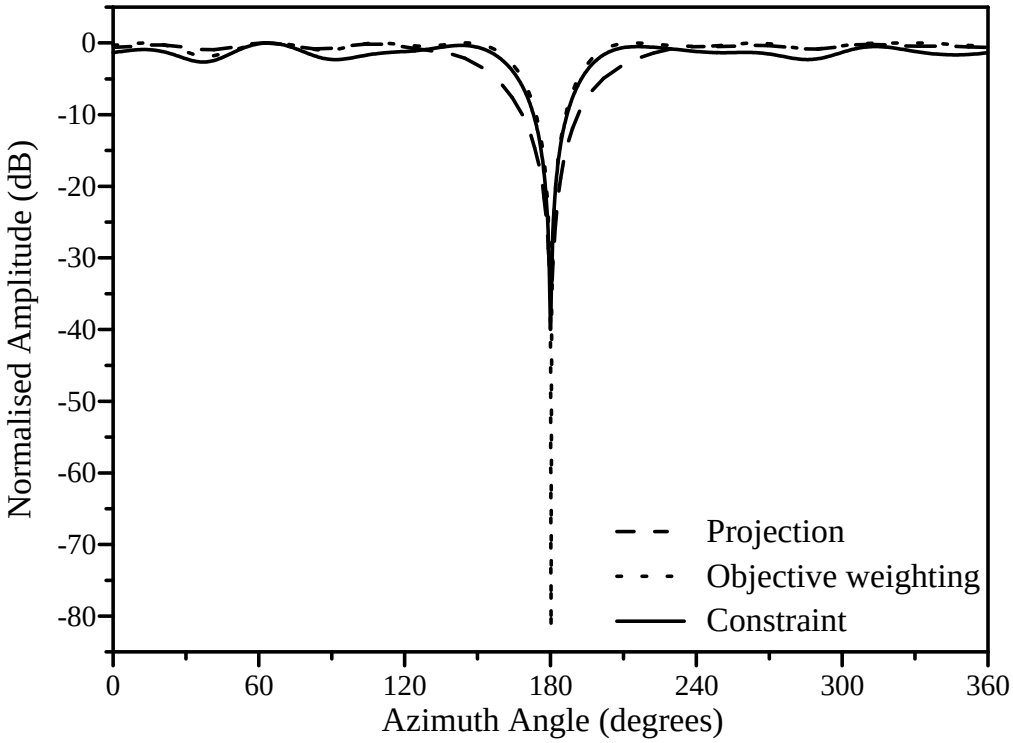

Figure 3.30: Radiation pattern of an axially polarised patch array (N=10 and $d_\phi = 0.5\lambda_0$) with a single null using different methods

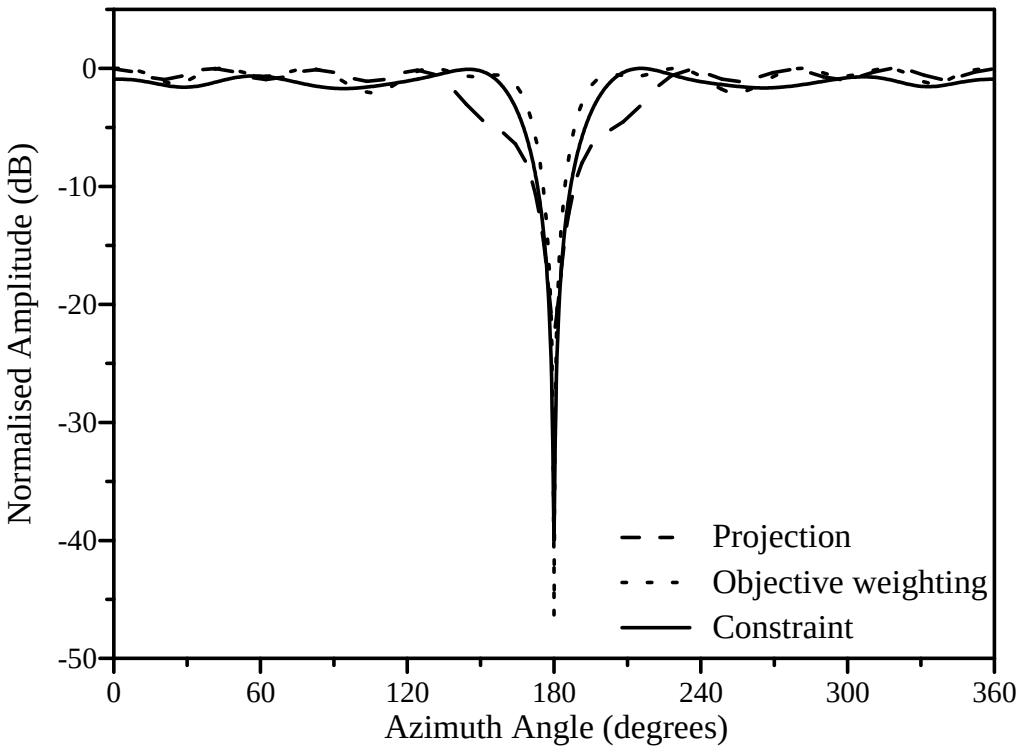

Figure 3.31: Radiation pattern of a cylindrical dipole array (N=10 and $d_\phi = 0.5\lambda_0$) with a single null using different methods

3.5 Multiple null synthesis

Where more than one interference should be suppressed, multiple null synthesis is required. The constrained optimisation method can be extended to perform the multiple null synthesis by adding the necessary constraints. The orthogonal projection method is used to obtain the optimum excitation vector, which is used as the starting vector for the optimisation.

In the first example, an omnidirectional radiation pattern with -40 dB nulls at 72° and 252° was specified. Constraints were specified for the two null depths as well as the ripple (1 dB or less). Figure 3.32 shows the amplitude pattern formed by the resulting excitation vector. The two nulls are present at the desired locations while the specified constraints are satisfied. Three -40 dB nulls were desired in the second example at 90°, 180° and 270°. A third constraint was added to the optimisation method for the additional null and the resulting amplitude pattern is shown in Figure 3.33. The pattern contains all three nulls at the specified locations with the desired null depths (-40 dB) and gain ripple (1 dB) between the nulls.

Cases with variable null depths were also studied. Firstly, two nulls were desired at 72° and 252° with null depths of -10 dB and -20 dB, respectively. The orthogonal projection method with the necessary variable phase steps in the idealised pattern was applied to form the starting excitation vector for the optimisation. The resulting radiation pattern is shown in Figure 3.34. The pattern contains the nulls with the desired null depths at the specified locations and the gain ripple is equal to 1 dB. An omnidirectional pattern containing three nulls with different null depths was also required. The nulls were desired at 90°, 180° and 270° with null depths of -10 dB, -15 dB and -20 dB, respectively. Figure 3.35 presents the resulting pattern with the three nulls at their desired locations. The null depths and gain ripple (1 dB) meet the required specifications.

The constrained optimisation method is thus able to form multiple nulls with different null depths while constraining the gain ripple in the omni-region. Since the null depths and ripple can be controlled, these characteristics are independent of the number of elements and the inter-element spacing. The null widths of the multiple nulls will, however, vary with the number of elements and inter-element spacing if they are not constrained as well.

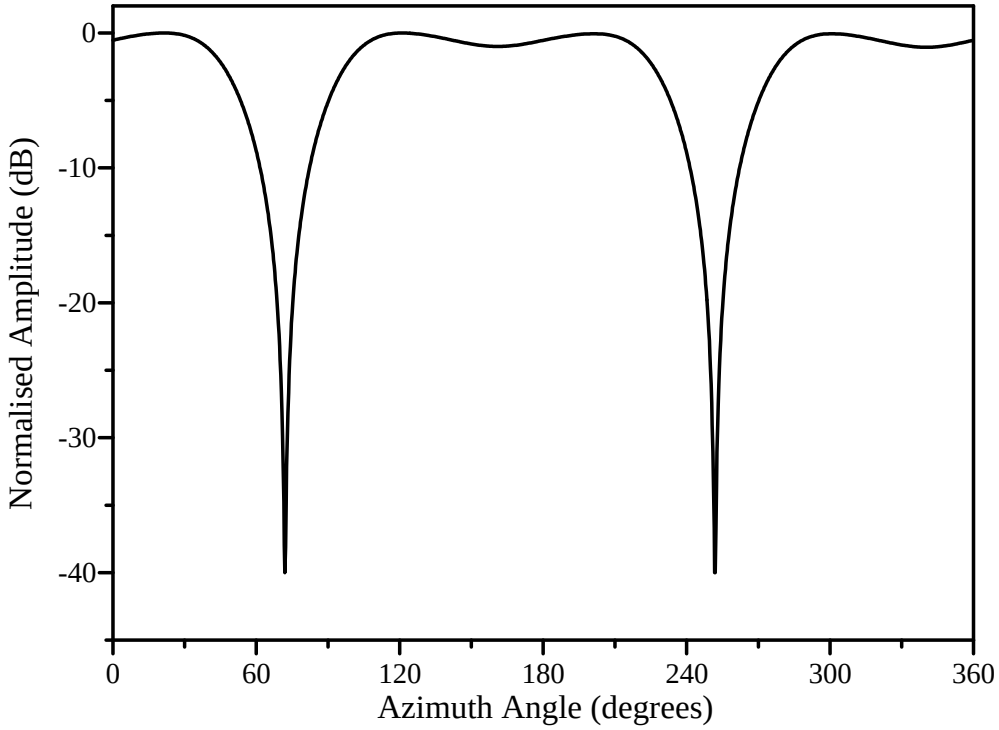

Figure 3.32: Radiation pattern of a circumferentially polarised patch array (N=10 and $d_\phi = 0.5\lambda_0$) with two nulls (72° and 252°), using constrained optimisation

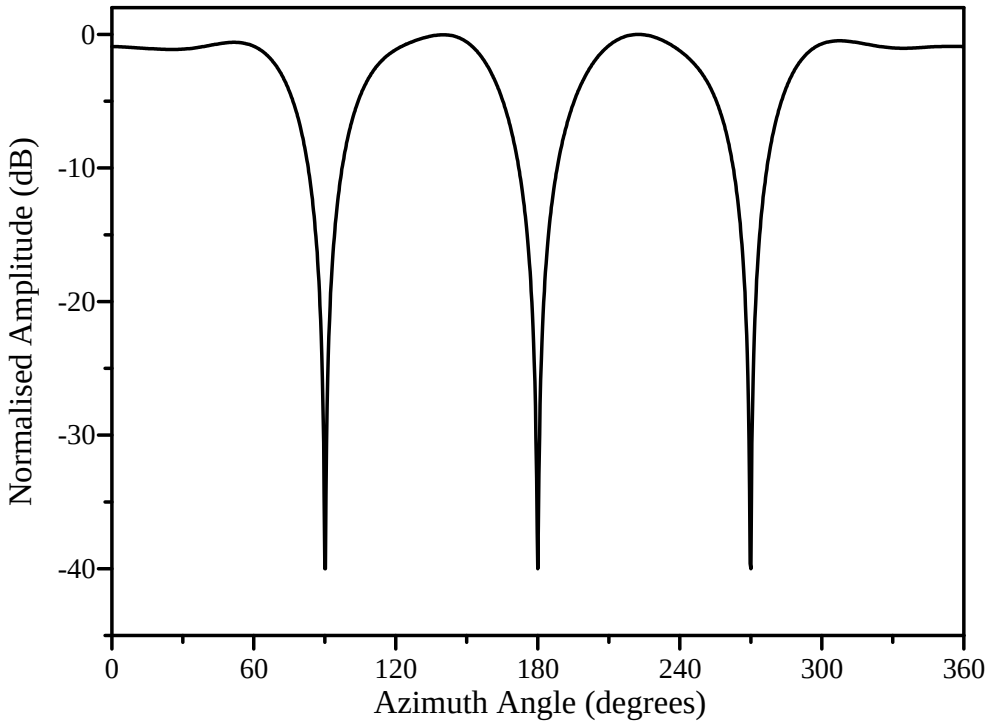

Figure 3.33: Radiation pattern of a circumferentially polarised patch array (N=10 and $d_\phi = 0.5\lambda_0$) with three nulls (90°, 180° and 270°), using constrained optimisation

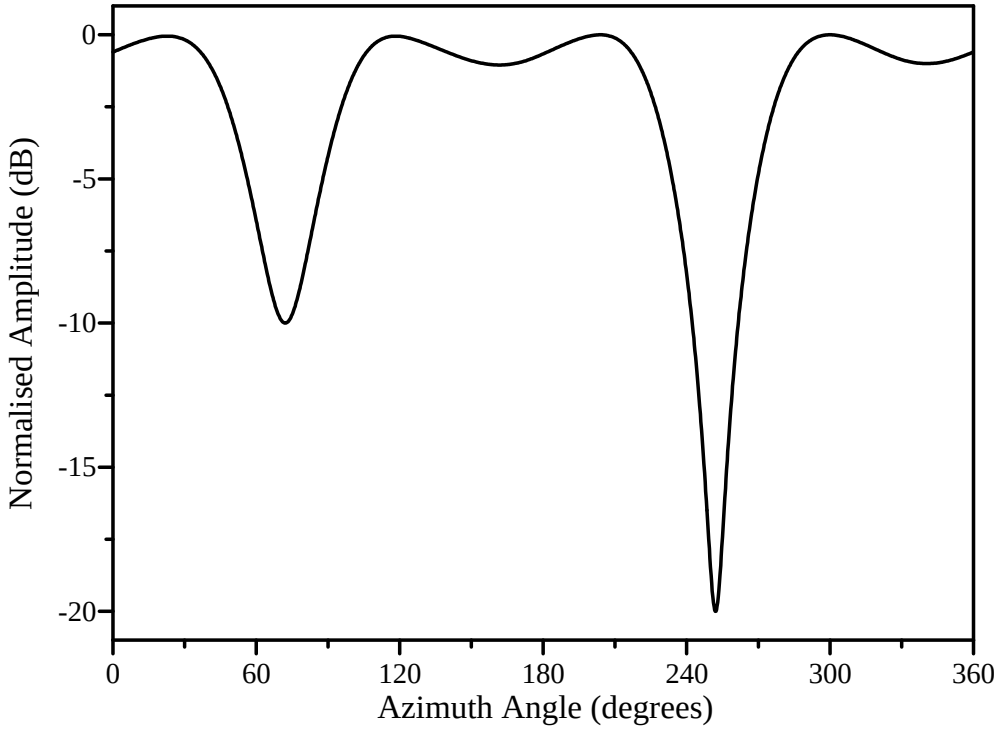

Figure 3.34: Radiation pattern of a circumferentially polarised patch array (N=10 and $d_\phi = 0.5\lambda_0$) with two nulls (72° and 252°), using constrained optimisation

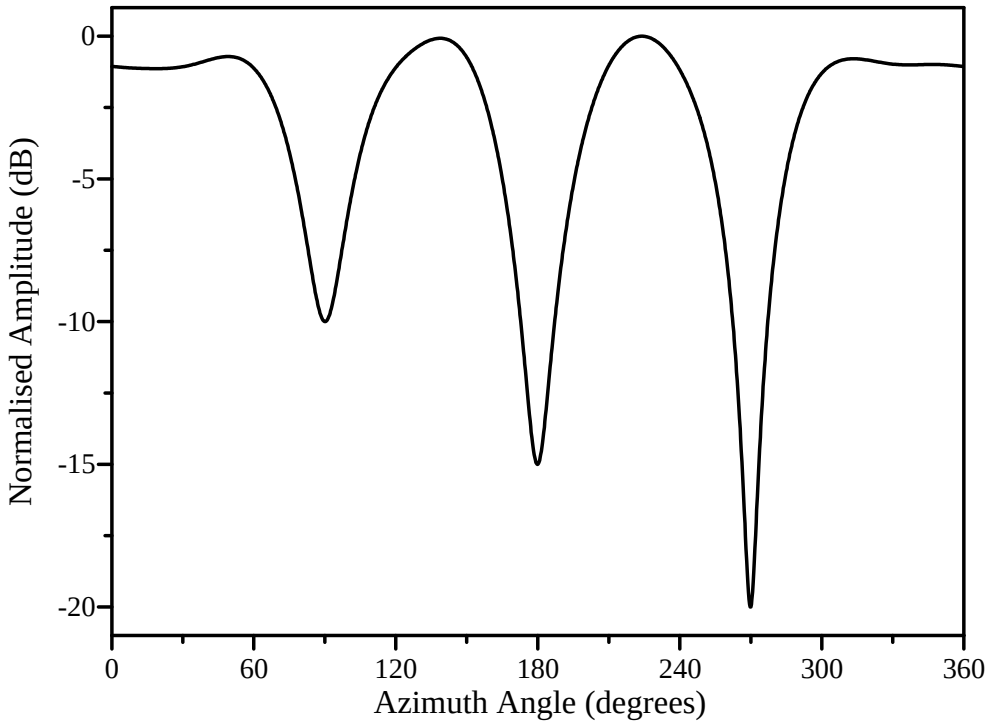

Figure 3.35: Radiation pattern of a circumferentially polarised patch array (N=10 and $d_\phi = 0.5\lambda_0$) with three nulls (90°, 180° and 270°), using constrained optimisation

3.6 Influences of the antenna element characteristics

The characteristics of the resulting null pattern may be influenced by the characteristics of the array as well as the attributes of the antenna element. The influence of the array characteristics such as the number of elements and the inter-element spacing have been shown in Section 3.3.1. Since the antenna element pattern varies with the height of the patch and the dielectric constant of the substrate, the resulting null pattern may also change due to variations in these characteristics. Different patch antenna elements were used to study the effects of element characteristics on the resulting null pattern.

3.6.1 Influence of the dielectric constant

Three different cylindrical patch antennas were designed to study the influence of using substrates with different dielectric constants. All three patches were designed for a resonant frequency of 1.8 GHz for the dominant mode and had a substrate height of $h = 1.6$ cm. For the first patch antenna, air was used as the substrate ($\varepsilon_r = 1$). The dimensions were $L = 7.97$ cm and $W = 8.2$ cm for the axial polarisation and vice versa for the circumferential polarisation. A substrate with $\varepsilon_r = 4.4$ was used to design the second patch antenna with dimensions of $L = 3.87$ cm and $W = 4.75$ cm for the axial polarisation; for the circumferential polarisation $W = 3.87$ cm and $L = 4.75$ cm. The results using these two patch antenna elements were compared with the results in the previous sections using the patch antenna with $\varepsilon_r = 2.3$ ($L = 5.44$ cm and $W = 6$ cm).

An omnidirectional pattern with a single null of -40 dB at 180° was specified. In each case the orthogonal base was modified to include the radiation pattern of the specific patch antenna element. Firstly, the constrained optimisation method was used without constraining the gain ripple. Figures 3.36 and 3.37 compare the amplitudes of resulting radiation patterns for the circumferential and axial polarisation, respectively. The axially polarised array using the air substrate forms the widest null with the most gain ripple. The other two axially polarised arrays form nulls with similar characteristics. The null width is almost the same for all three axial polarisation cases. For the circumferential polarisation, the resulting pattern of the array using the substrate with $\varepsilon_r = 4.4$ has the highest gain ripple. The null widths of all three patterns differ by less

than 0.5°.

The ripple was also constrained (1 dB or less) to yield the resulting patterns in Figures 3.38 and 3.39 for the circumferential and axial polarisation, respectively. In the circumferential and axial polarisations, the air substrate array produces the widest and narrowest nulls, respectively. On the other hand, the array with the $\varepsilon_r = 4.4$ substrate, yields the narrowest and widest nulls in the circumferential and axial polarisations, respectively. From these results, it can be concluded that the choice of the dielectric constant of the substrate will have an effect on the resulting null pattern characteristics. This is mainly due to the differences in element patterns when using different substrates.

3.6.2 Influence of the height of the substrate

Another attribute of the patch antenna elements which modifies the element pattern, is the height of the substrate. Two patch antenna elements with different heights were used to illustrate the influence of the height of the substrate. A foam based substrate with $\varepsilon_r = 1.024$ was used to design the two patches with $h = 1.6$ mm and $h = 5$ mm, respectively. Both patches were designed for a resonant frequency of 1.8 GHz. The dimensions for both patches were $L = 7.36$ cm and $W = 7.6$ cm for the axial polarisation and vice versa for the circumferential polarisation. The cavity model was used to obtain the element pattern of the patch with $h = 1.6$ mm. For the patch with $h = 5$ mm, a FDTD software package [101] was used to compute the element pattern.

The constrained optimisation method was used to determine the excitation vectors for a -40 dB null at 180°. Figures 3.40 and 3.41 compare the amplitude of the resulting radiated fields when only the null depth is constrained for the circumferential and axial polarisations, respectively. For $h = 5$ mm, a wider null with a higher gain ripple is formed for the circumferential polarisation. In contrast, the results are very similar when the two axial polarisation patterns are compared. When the gain ripple is constrained to 1dB or less, the resulting amplitude pattern in Figures 3.42 and 3.43 are obtained for the circumferential and axial polarisations, respectively.

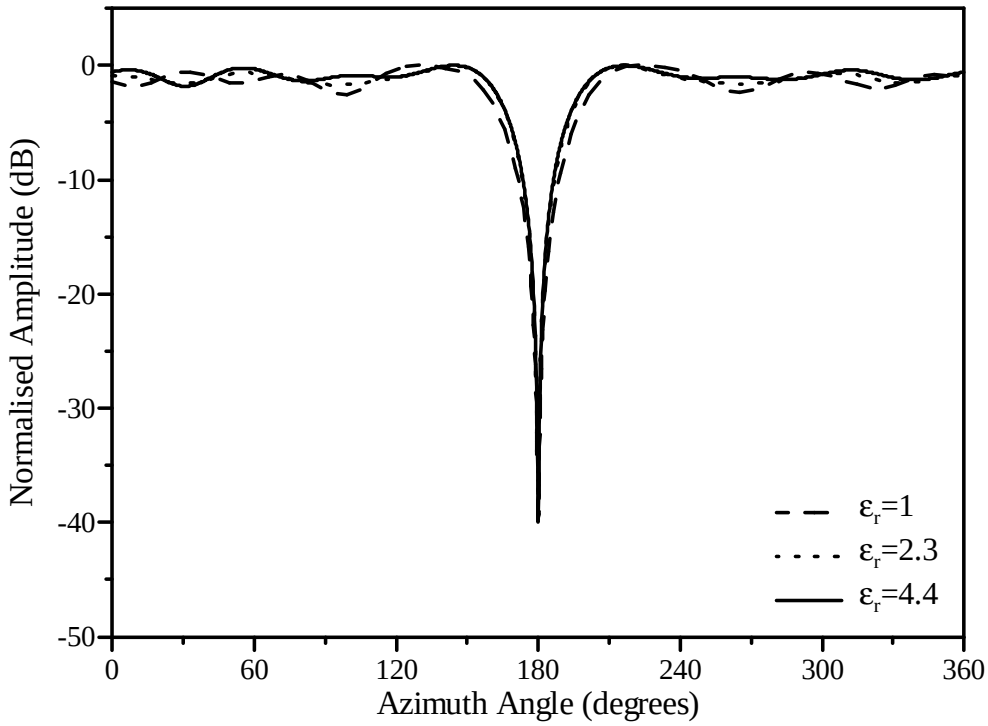

Figure 3.36: Comparison of the radiation patterns of circumferentially polarised patch arrays (N=10 and $d_\phi = 0.5\lambda_0$) using antenna elements with different substrates

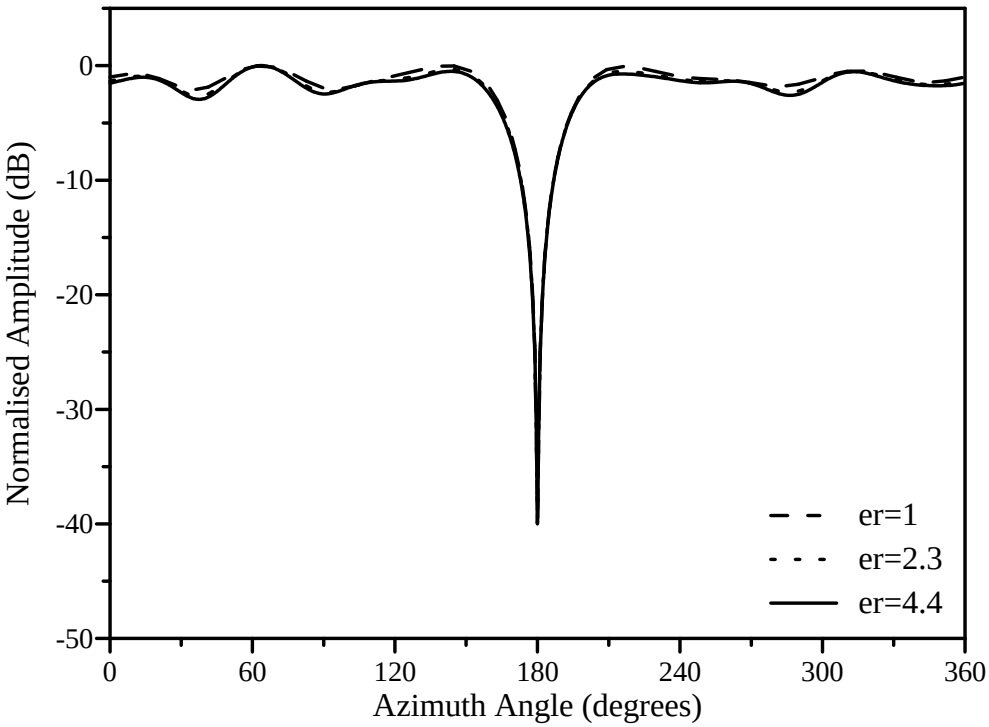

Figure 3.37: Comparison of the radiation patterns of axially polarised patch arrays (N=10 and $d_\phi = 0.5\lambda_0$) using antenna elements with different substrates

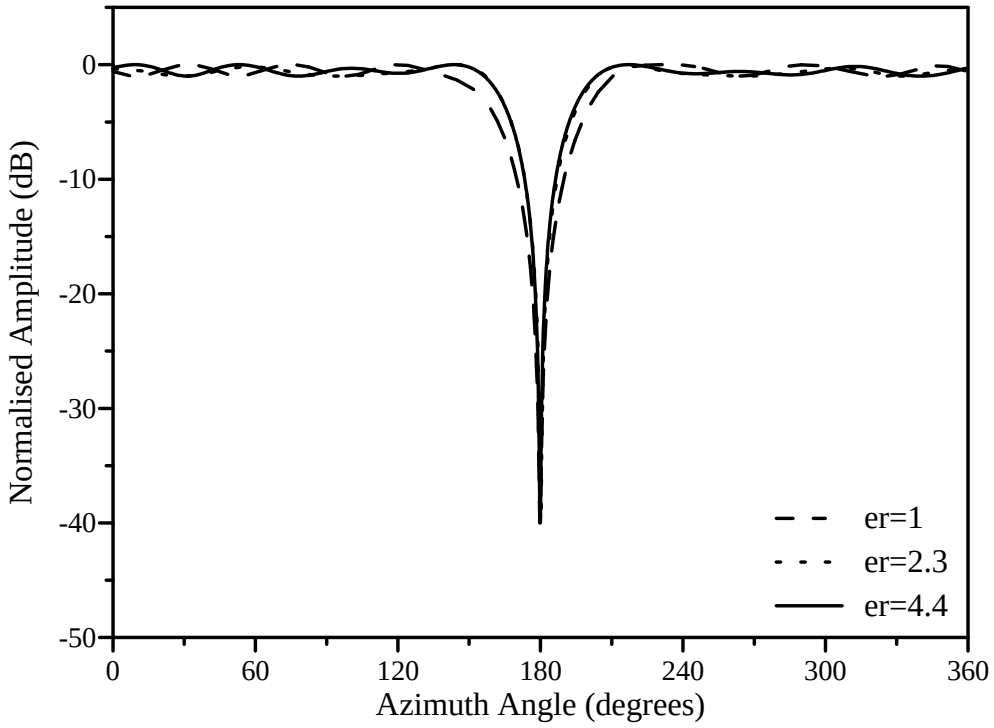

Figure 3.38: Comparison of the radiation patterns of circumferentially polarised patch arrays (N=10 and $d_\phi = 0.5\lambda_0$) using antenna elements with different substrates

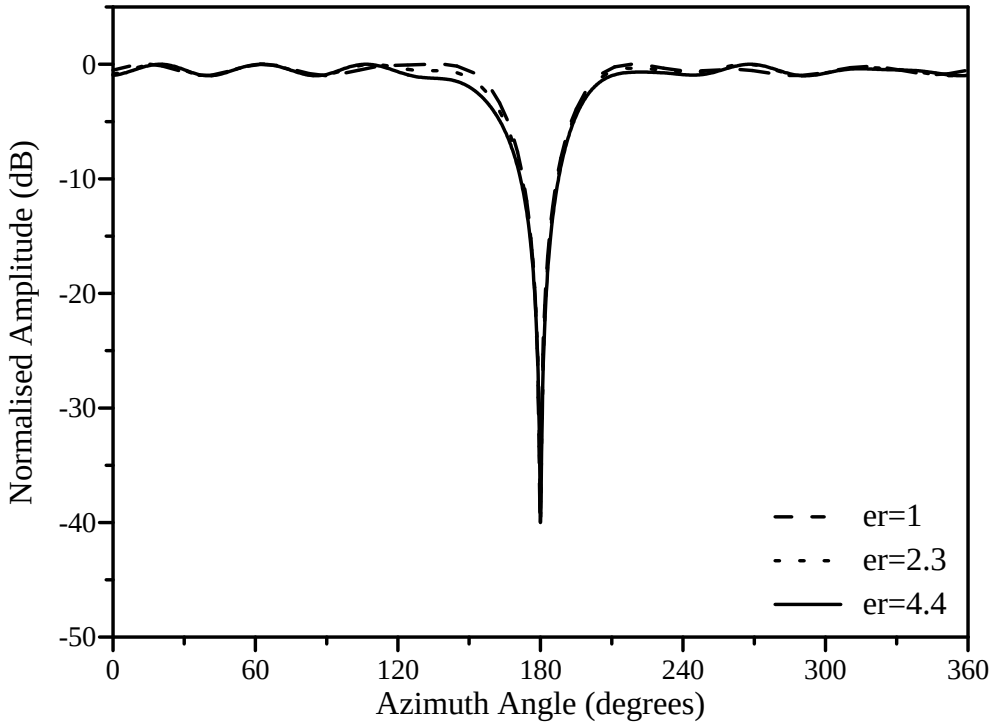

Figure 3.39: Comparison of the radiation patterns of axially polarised patch arrays (N=10 and $d_\phi = 0.5\lambda_0$) using antenna elements with different substrates

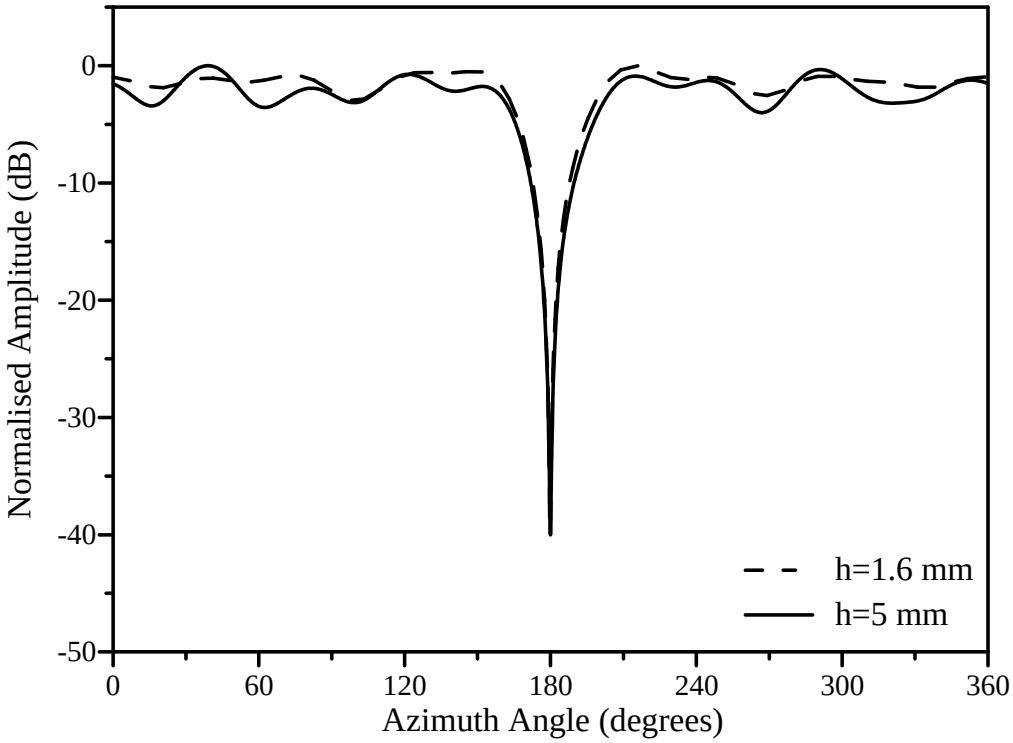

Figure 3.40: Comparison of the radiation patterns of circumferentially polarised patch arrays (N=10 and $d_\phi = 0.5\lambda_0$) using antenna elements with different substrate heights

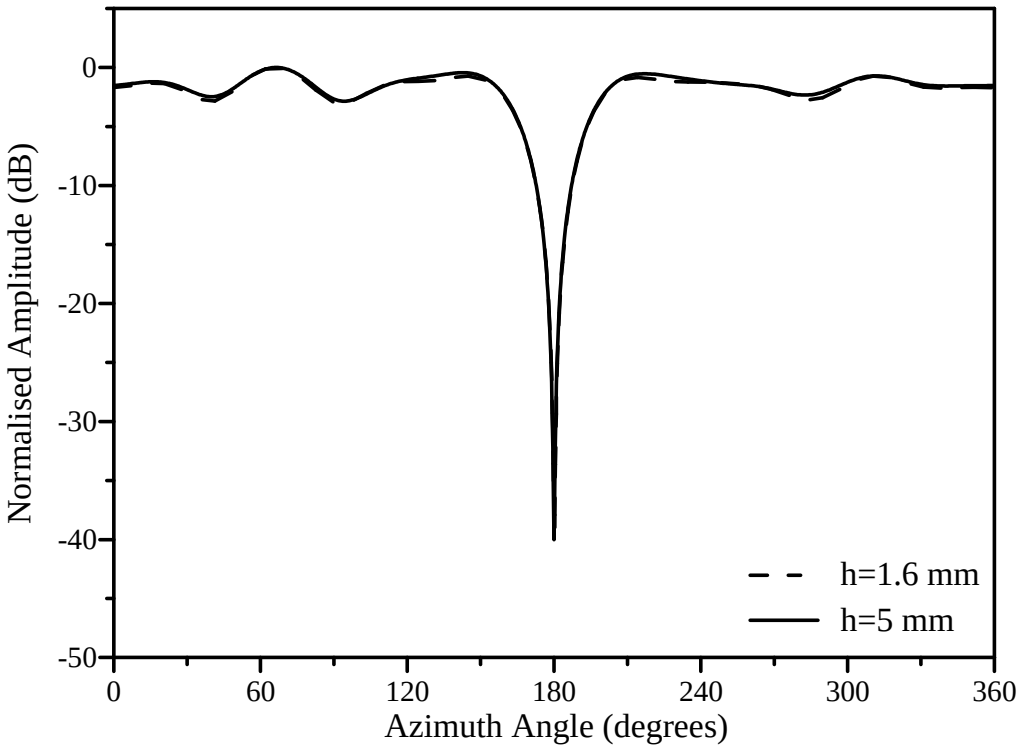

Figure 3.41: Comparison of the radiation patterns of axially polarised patch arrays (N=10 and $d_\phi = 0.5\lambda_0$) using antenna elements with different substrate heights

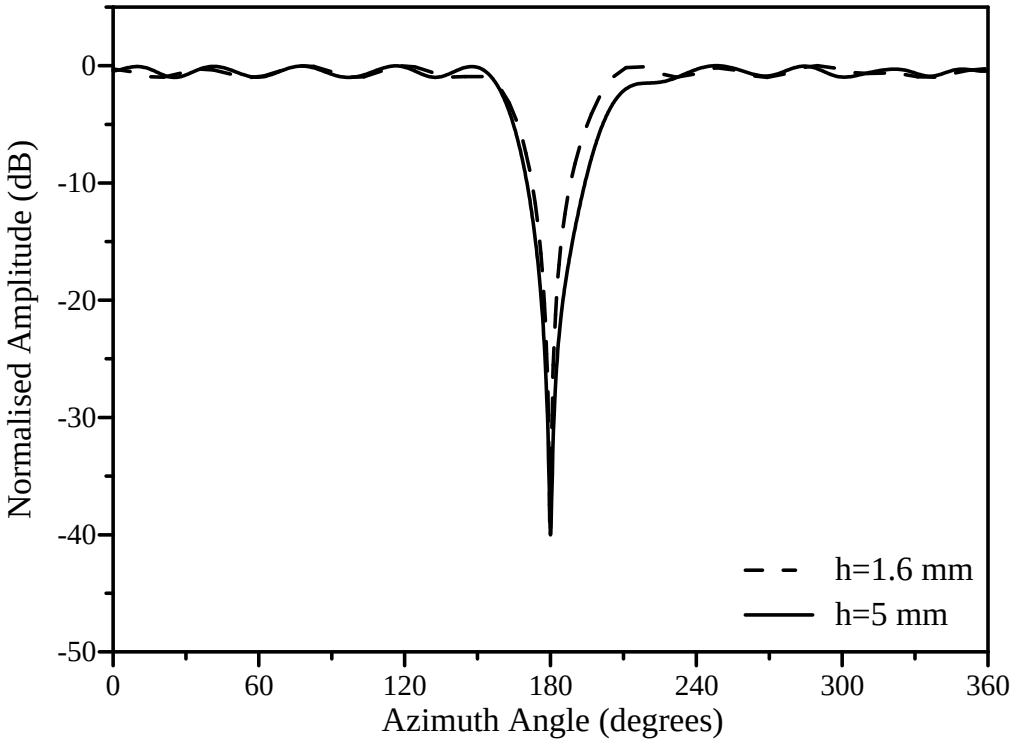

Figure 3.42: Comparison of the radiation patterns of circumferentially polarised patch arrays (N=10 and $d_\phi = 0.5\lambda_0$) using antenna elements with different substrate heights

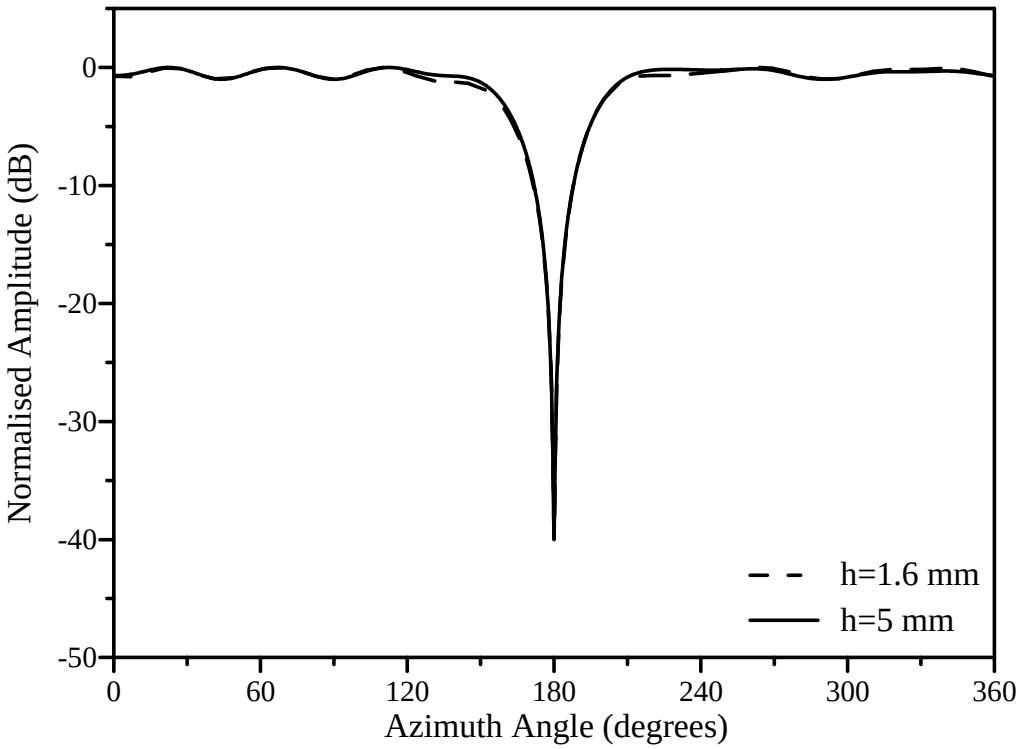

Figure 3.43: Comparison of the radiation patterns of axially polarised patch arrays (N=10 and $d_\phi = 0.5\lambda_0$) using antenna elements with different substrate heights

A null width difference of 7.04° exists between the two resulting circumferential polarisation patterns with the pattern for $h = 5$ mm having the widest null. The axial polarisation patterns differ only slightly. The choice of the substrate height has a greater influence on the resulting null width and gain ripple in the circumferential polarisation, since the element patterns for this polarisation differ more for different substrate heights. For this polarisation, a low substrate height is recommended when a narrow null is preferred.

3.7 Results for various null positions

Depending on the available degrees of freedom, the resulting characteristics of a null pattern may vary as the angular position of the null is changed. When a large number of elements is used, the variation in the null pattern will be low. On the other hand, the variations in the pattern characteristics may be higher when a small number of elements is used.

To study the influence of the position of the null, a -40 dB null was formed at different angular positions using patch arrays with N=10 and $d_\phi = 0.5\lambda_0$. Table 3.3 compares the resulting null pattern characteristics as the null position is varied for the different polarisations and the various constraints used in the constrained optimisation method. The angular position of the null is changed from ϕ_n to $\phi_n + \pi/N$ at 180° and 198°, respectively. The resulting amplitude patterns are compared in Figures 3.44 and 3.45 for circumferential and axial polarisations, respectively. These patterns are obtained when the null depth and the gain ripple are constrained to -40 dB and 1 dB, respectively.

The values of the pattern characteristics for a null at 180° and 198° do not differ much for the circumferential polarisation. Using this polarisation, the maximum gain ripple and null width occur when a null is desired at 189° ($\phi_n + \pi/2N$). When the axially polarised array is utilised and only the null depth is constrained, the gain ripple increases while the null width decreases as the null position is varied from 180° to 198°. A maximum null width is obtained at 198° when the gain ripple is constrained as well. In this case, the null width increased by 2.04° when the desired angular null position was changed from 180° to 198°.

Table 3.3: Results for cylindrical arrays with $N = 10$ and $d_\phi = 0.5\lambda_0$ using the constrained optimisation method for different null positions

Array type	**Constraints**	**Null position (°)**	**Ripple (dB)**	**Null width (°)**
Circumferentially polarised patches	-40 dB depth	180	1.70	13.54
		189	1.86	13.73
		198	1.72	13.47
	-40 dB depth 1dB ripple	180	1.00	13.58
		189	1.00	13.74
		198	1.00	13.55
Axially polarised patches	-40 dB depth	180	2.66	13.81
		189	2.72	13.49
		198	2.93	13.28
	-40 dB depth 1dB ripple	180	1.00	15.25
		189	1.00	14.58
		198	1.00	17.29

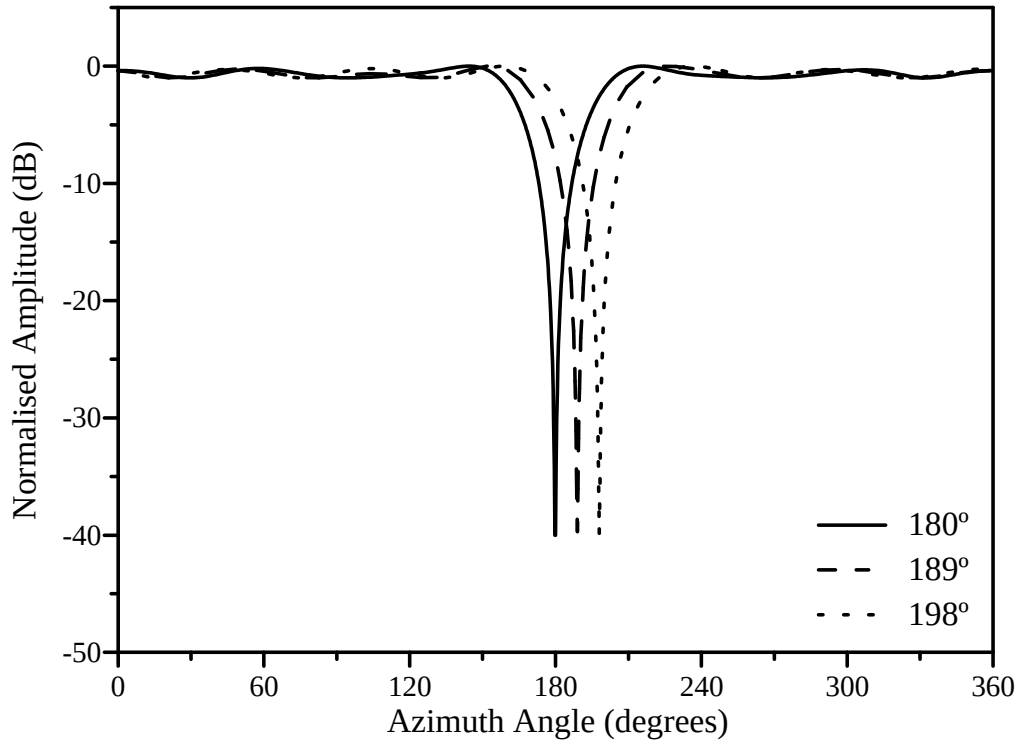

Figure 3.44: Comparison of the radiation patterns of a circumferentially polarised patch array (N=10 and $d_\phi = 0.5\lambda_0$) when the null position is varied

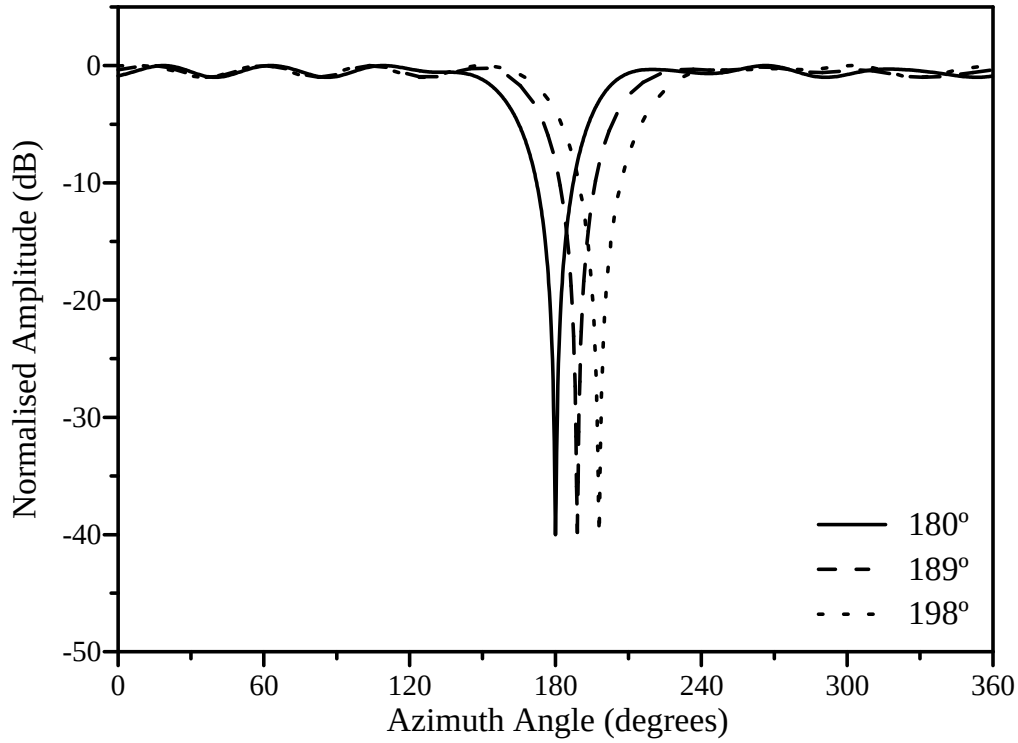

Figure 3.45: Comparison of the radiation patterns of an axially polarised patch array (N=10 and $d_\phi = 0.5\lambda_0$) when the null position is varied

The degree to which the characteristics of the resulting null pattern change as the null position is varied, depends on the utilised polarisation. The variations in the pattern characteristics consequently depend on the element pattern that is incorporated. By carefull selection of the element pattern, the sensitivity of the pattern characteristics to a change in the null position, can thus be minimised.

3.8 Summary

Abele *et al.* [53] introduced a null synthesis technique for a cylindrical dipole array. The technique utilised the orthogonal projection method and projected an idealised null pattern onto the orthogonal base of realisable array patterns. The resulting array pattern was an omni-directional pattern with one or more nulls. Vescovo [56] extended the orthogonal projection method for an arc array with theoretical directional elements. A beam pattern was formed through the projection method and additional nulls were introduced in the pattern with null constraints to reduce the side lobe level. In this chapter the null synthesis technique of Abele was extended to incorporate the radiation

patterns of conformal microstrip patches.

In this chapter, the null synthesis technique of Abele [53] was used to form an omnidirectional radiation pattern with nulls at specified locations for a cylindrical microstrip patch array. The orthogonal projection method was extended by modifying the orthogonal base for the space of realisable array pattern to include the radiation pattern characteristics of microstrip patch antennae mounted on a conducting cylinder. For electrically thin patches, the cavity model was used to compute the element pattern of the cylindrical patches. A FDTD software package [101] was used to calculate the element pattern of electrically thick cylindrical patches. The unconstrained optimum element excitations obtained from the orthogonal projection method provided an optimal array pattern with the minimum pattern error (in a least square sense).

The resulting radiation pattern contained the desired null at the specified angular location in the otherwise omnidirectional pattern. By applying a Hamming window to the sequence excitations before the element excitations are computed, the gain ripple in the omniregion was reduced. The resulting null pattern characteristics were also influenced by the array configuration parameters such as the number of elements and the inter-element spacing. When an infinitely deep null was desired, the resulting gain ripple and null width gradually decreased while the null depth increases as the number of elements were increased for both axially and circumferentially polarised microstrip patch arrays. As the inter-element spacing was increased, the gain ripple and null width increased as well. For a large number of elements the yielded null widths became comparable to the null widths obtained with dipoles as the array elements. In most cases, the microstrip patches yielded better gain ripple due to the high level of gain ripple in the radiated field of cylindrical dipole arrays.

Since the amplitude and phase of the radiation pattern were optimised simultaneously, the optimal array pattern may not have had the desired characteristics. Although the ripple was successfully decreased by using the windowing function, the resulting null width was increased. Instead of only minimising the array pattern error, a multi-objective optimisation approach was followed [95–97]. The Objective Weighting method, previously applied in other fields of computational electromagnetic problems [96, 97], was used to improve the amplitude pattern characteristics. A global performance function was defined by utilising both the amplitude pattern error and the phase pattern error. The optimisation problem was solved by finding the critical

ratio of the weights that were assigned to the two errors in the performance function. Each performance function was minimised by using an unconstrained minimisation algorithm [99]. The excitation vector obtained from the orthogonal projection method yielded an optimum radiation pattern with the minimum pattern error and was therefore chosen as the starting vector. The resulting excitation vector that minimised the performance function formed with the critical weight ratio, was used to form the radiation pattern.

Compared to the results of the windowing method, the objective weighting method provided a null pattern with a narrower and deeper null and with a higher gain ripple in the omni-region. An increase in the phase pattern error was observed due to the trade-off that existed between the two pattern errors in the performance function. When infinitely deep nulls were desired, the method could synthesise deep nulls utilising only a small number of elements.

Constrained optimisation methods have been used previously to form beam patterns with cylindrical arrays [45, 52, 56]. Prasad [45] applied the least squares optimisation method to circular and arc arrays to form a beam pattern with a specified beamwidth. Additional nulls were also placed in the sidelobe region by using null constraints while minimising the mean square difference between the desired pattern and the optimum pattern. The Hook and Jeeves algorithm was also used to perform an iterative search to find the optimum excitation vector while satisfying the null constraints. During the search, the sidelobe level was minimised. Ares *et al.* [52] used a simulated annealing technique to produce beam patterns for a circular arc array on a cylinder. A cost function, which could include terms to control the radiation pattern, was minimised. Terms which placed constraints on the excitations, could also be included in the cost function. The sidelobe level was also decreased by placing null constraints in the region near the main lobe [56]. In this chapter, constrained optimisation was also used to yield an excitation vector which minimises the pattern error under the constraints specified for the different amplitude pattern characteristics. The minimum pattern error was found using a constrained minimisation algorithm [99]. The optimum element excitation vector, which was obtained from the projection method, was used as the starting vector.

Individual characteristics as well as combinations of characteristics were controlled using the constrained optimisation. Compared to the above methods, the constrained

optimisation algorithm obtained a null width close to the null width resulting from the objective weighting method, while controlling both the null depth and gain ripple in the omni-region. The method was also able to form multiple nulls with different null depths while constraining the gain ripple. Due to the control provided by the algorithm, the resulting pattern characteristics could be made independent of the number of elements and the inter-element spacing.

Since the element pattern can not be factorised out of the array factor, any change in the element pattern may influence the characteristics of the resulting array pattern. While controlling certain null pattern characteristics, the influence of changes in the antenna element configuration on the remaining unconstrained pattern characteristics, was studied. The effects of the changes in the dielectric constant and the height of the substrate are different for the circumferentially and axially polarisations. The null pattern characteristics for the axial polarisation are only slightly influenced by a change in substrate height. When the null depth is constrained, the resulting ripple and null width for both polarisations are influenced by a change in the dielectric constant. The degree to which the unconstrained characteristics of the resulting null pattern change as the null position is varied, also depend on the utilised polarisation. The sensitivity of the resulting null pattern characteristics to a change in the desired null position or an antenna element characteristic, can be minimised by a careful selection of the element pattern.

The above three null synthesis methods determines the necessary element excitations without considering the mutual coupling between the elements. If the inter-element spacing is chosen large enough or the height of the patch elements is low in terms of wavelength, the mutual coupling factor is small and has very little effect on the resulting pattern. On the other hand, the mutual coupling between closely spaced patch antenna elements with high substrate heights, is large enough to distort the resulting radiation pattern. Consequently, the mutual coupling must be compensated for. In most systems, the driving impedances of the patch antenna elements also need to be matched to the input system. In the next chapter, a mutual coupling compensation technique is employed which alter the patch antenna element geometries to simultaneously correct the resulting null pattern and the driving impedances of the antenna elements.